Multidimensional Fourier spectroscopy of semiconductors. I. Nonequilibrium Green function approach

Kuljit S. Virk* and J. E. Sipe†
Department of Physics and Institute for Optical Sciences, University of Toronto, 60 St. George Street, Toronto, Ontario, Canada M5S 1A7

(Received 3 October 2008; revised manuscript received 6 July 2009; published 15 October 2009)

We develop a framework for describing the two-dimensional Fourier spectroscopy of semiconductors based on nonequilibrium Green functions. A perturbative treatment of the electromagnetic field is used to derive a closed set of differential equations for the multiparticle correlation functions, which take into account the many-body effects up to the third order in the field. A diagrammatic method is also developed to describe the driving of the many-body system by the three optical pulses. The method retains all features of the double-sided Feynman diagrams for bookkeeping the excitation scenario, and complements it by allowing for the description of interactions as well. Rules for the diagrams are also derived.

DOI: 10.1103/PhysRevB.80.165318 PACS number(s): 78.47.−p, 78.67.−n, 42.50.Md, 78.20.Bh

I. INTRODUCTION

Decoherence plays a central role in both fundamental quantum theory and in applications to quantum information processing. The phenomenon of decoherence also serves as a window on the dynamics of complex systems. Among the richest venues for the study of dynamics of complex interacting systems are semiconductors and their nanostructures. Optical excitation and probing of these systems with ultrashort pulses allows us to study their dynamics at ever decreasing time scales. However, this dynamics is so complex that it has not been fully elucidated experimentally or theoretically. This is partly due to the similar time scales of many interaction processes, which require severe approximations in theory, and partly due to the limitations of experimental techniques in separating the different contributions to the signal.

Two-dimensional Fourier spectroscopy (TDFS), an experimental technique that has played a key role in NMR and molecular chemistry, is now offering exciting prospects for probing the dynamics of semiconductor systems.[1–3] The distinguishing aspect of this technique is the excitation of the system by three phase-locked pulses, separated by controllable time delays. Their combined effect on the evolution of the system leads to a signal propagating in a background-free direction. A measurement of its phase and magnitude allows one to construct the two-particle correlations. The construction can then be Fourier transformed, and various excitations and coherences can be separated spectrally, and spatially via selecting appropriate directions for the exciting pulses.[4] This unprecedented control over excitations, and extraction of information from the signal leads to a much more detailed picture of ultrafast dynamics than previously available.

Experimental probes such as TDFS are perhaps most useful in the weak-field limit, because perturbation theory can be used to identify the dominant contributions to the signal, with the nth order susceptibility $\chi^{(n)}$ of the system describing the response to an excitation by n pulses. The variations of the signal as the temporal delays between the pulses are changed then allows for the extraction of the dependence of $\chi^{(n)}$ on its different frequency components. Many of the theoretical treatments presented to date have relied on density matrix equations employing phenomenological parameters, with the solutions often illustrated by double-sided Feynman diagrams.[5] Remarkably powerful in identifying the underlying physical processes, they are not fundamental enough to allow comparison of detailed many-body theory with experiment.

Of the several approaches to a more fundamental, microscopic theory for $\chi^{(3)}$ in relation to four-wave mixing,[6–9] the most widely used has been dynamics controlled truncation (DCT), which falls in the category of density matrix many-body theory. It is based on a theorem by Axt and Stahl[8] that relates the expectation value of n electron/hole operators to the order n in the driving electric field. A severe restriction on the validity of the theorem is the assumption that the initial state is a semiconductor ground state of the Hartree-Fock type. Either a correlated ground state or the presence of initial carrier densities, both of which are feasible experimentally and often of primary interest, can be handled only by phenomenological extensions. At the most rigorous level it is also restricted to coherent dynamics because of the infinite partial summations involved in irreversible dynamics. An alternate approach developed in the extensive work by Kira *et al.*,[9] based on cluster expansions, formally circumvents all these limitations and in principle offers an exact theory for a wide class of problems. Yet in practical applications it involves a truncation in the cluster expansion, often in a way that does not allow a straightforward comparison with more phenomenological approaches and does not allow for the identification of terms particularly of interest for decoherence.

The response of a semiconductor to optical pulses has also been studied within the framework of Green function theory, with a link between DCT and the Green function approach established by Kwong *et al.*[10] The work by Schafer *et al.*,[6] based on a Green function formalism developed from functional differentiation, is a benchmark in this field. But in separating the even and odd orders of the field it relies on the assumption of a slowly varying single pulse, and is not aimed at extracting a $\chi^{(3)}$. With the aim of addressing TDFS experiments, the approach of Maialle *et al.*[7] involves con-

structing the $\chi^{(3)}$ response from electron and hole Green functions, dressed by Coulomb interactions. While providing a physical picture of the basic interaction processes, it has been developed only as far as the assumptions of DCT, with diagram rules that allow for only bare Coulomb interaction, assume an initial state of zero density, and stay within a two-band model of the semiconductor. In addition, any decoherence effects are only captured using a set of constant rates for different quasiparticles.

Here we develop a more general theoretical approach for constructing the $\chi^{(n)}$ response, within the framework of nonequilibrium Green functions. In this initial work we neglect phonons and restrict ourselves solely to interacting charged particles in the presence of a lattice potential. The fundamental entity here is the single-particle Green function G, which can be used to calculate the charge-current density that is the source of the signal in a TDFS experiment. In this approach, which is not restricted to an uncorrelated initial state, the expansion of the response in terms of susceptibilities $\chi^{(n)}$ is accomplished by developing an expansion for changes ΔG to G in terms of quantities $\mathfrak{X}_n^{(1)}$, $\Delta G=\mathfrak{X}_1^{(1)}+\mathfrak{X}_2^{(1)}+\mathfrak{X}_3^{(1)}+\cdots$, where each term involves a higher power of the full incident field. The inevitable hierarchy that arises in many-body physics here manifests itself in the coupling of the $\mathfrak{X}_n^{(1)}$ to higher correlations $\mathfrak{X}_n^{(j)}$, with $j>1$. Different dynamical models are associated with different approximations of this hierarchy, corresponding to approximations to vertex functions or, equivalently, with sets of diagrams kept in the expansion of the self-energy. Thus the physics of any adopted approximations can be identified. We develop a truncation scheme particularly suited to the perturbative response characteristic of TDFS. This is essential. To treat decoherence effects properly, we must go beyond treatments of the type of Schafer *et al.*[6] that include only screened Hartree-Fock theory, extended to the ladder approximation of a Bethe-Salpeter equation to account for excitons.

The quantities $\mathfrak{X}_n^{(j)}$ satisfy equations of motion that couple them to each other and to source terms. They also have a diagrammatic expansion that parallels the kind of double-sided Feynman diagrams familiar from more phenomenological approaches. Thus we can establish a link with simpler treatments, of which ours can be considered a generalization. Perhaps even most importantly, a new perspective on decoherence arises naturally from this work. In many treatments, decoherence arises in a system interacting with a reservoir, and appears formally when the reservoir is traced over to yield a reduced density operator that then characterizes the results of measurements on the system. The approach presented here is necessarily much more general since, due to the indistinguishability of electrons, no formal factorization of the Hilbert space into "system" and "reservoir" is possible. Here decoherence as a phenomenon can be associated with the fact that our experiments are sensitive only to $\mathfrak{X}_n^{(1)}$, and not to the higher order $\mathfrak{X}_n^{(j)}$, $j>1$. Experimental consequences of these higher $\mathfrak{X}_n^{(j)}$ arise only insofar as they affect the dynamics of $\mathfrak{X}_n^{(1)}$. While this parallels the simpler situation where there is a well-defined system and reservoir, and experimental consequences of the reservoir arise only insofar as the reservoir affects the dynamics of the reduced density operator of the system, it offers a broader view and allows for a richer perspective on what are phenomenologically called "decoherence effects." We plan to turn to elaborations of this perspective in future publications, the first of which is the paper following (referred to as II hereafter).

In this first paper we focus on the development of this approach to Fourier transform spectroscopy based on nonequilibrium Green functions. In Sec. II we describe the Hamiltonian, and discuss how we specialize the existing general formalism of nonequilibrium Green functions to describe the nonlinear optical response in TDFS. In Sec. III we discuss the expansion of ΔG and address the hierarchy problem of multiparticle correlations. We end that section with a derivation of the equations of motion for $\mathfrak{X}_n^{(j)}$. Finally, in Sec. IV, we develop the diagram method as a general bookkeeping device. We then illustrate the main points of the formalism by determining the TDFS signal (leaving all details to II) for specific pulse sequence leading to coherence among exciton states. Here we also extend the diagram method as a tool for building approximate solutions, which is useful at least in specific cases. In II we present, as a first application of this approach and a topic of interest in its own right, the effect of decoherence between optically excited exciton states. We derive dynamical equations and compare and contrast them with those for the interband polarization. Thus II also identifies some of the main features of the general formalism within a specific calculation.

II. THEORETICAL BACKGROUND

A. Hamiltonian

In a two-dimensional Fourier spectroscopy experiment there are three pulses incident on the target material, which for the moment we take to be a single quantum well embedded in a semiconductor with a background relative dielectric constant ε that is real and positive. We describe these pulses classically, and write the electric fields associated with them as $\boldsymbol{E}_a(\boldsymbol{r},t)$, $\boldsymbol{E}_b(\boldsymbol{r},t)$, and $\boldsymbol{E}_c(\boldsymbol{r},t)$. The total incident field on the quantum well, with its growth axis taken to be the z axis and centered at $z=0$, is then

$$\boldsymbol{E}_{inc}(\boldsymbol{r},t)=\boldsymbol{E}_a(\boldsymbol{r},t)+\boldsymbol{E}_b(\boldsymbol{r},t)+\boldsymbol{E}_c(\boldsymbol{r},t). \tag{1}$$

Our goal is to calculate the response of the expectation values of the charge density operator and the current density operator, $\langle\rho(\boldsymbol{r},t)\rangle$ and $\langle\boldsymbol{J}(\boldsymbol{r},t)\rangle$, respectively; these will be perturbed from their equilibrium values in the neighborhood of the quantum well. These expectation values are then taken, in the usual semiclassical manner, as the source of the generated signal $\boldsymbol{E}_d(\boldsymbol{r},t)$. The problem is simplified because the thickness of the quantum well is much less than the wavelength of light, and the variation of the expectation value of electromagnetic field in the plane of the quantum well, which arises because the pulses will not all be normally incident on the well, will be over distances large compared to the thickness of the well. Within these approximations, we argue in Appendix A that we can calculate $\langle\bar{\rho}(\boldsymbol{r},t)\rangle$ and $\langle\bar{\boldsymbol{J}}(\boldsymbol{r},t)\rangle$ at a given $(x_o y_o)$, where the overbar indicates an average over the lattice spacing, by calculating the response of a quantum well to a field described by a nominal uniform

vector potential $\boldsymbol{A}_{nom}(t)$. That nominal vector potential takes the value that an effective vector potential actually takes at $(x_o y_o)$, where the effective vector potential is essentially uniform along z and includes contributions from the incident fields and the transverse field from the quantum well itself. Hence the many-body problem we must address involves the Hamiltonian

$$\mathcal{H}(t) = \frac{1}{2m}\int \left[\left(\frac{\hbar}{i}\nabla - e\boldsymbol{A}_{nom}(t)\right)\psi(\boldsymbol{r})\right]^{\dagger} \times\left[\left(\frac{\hbar}{i}\nabla - e\boldsymbol{A}_{nom}(t)\right)\psi(\boldsymbol{r})\right]d\boldsymbol{r} + \int v_0(\boldsymbol{r})\psi^{\dagger}(\boldsymbol{r})\psi(\boldsymbol{r})d\boldsymbol{r} + \int \psi^{\dagger}(\boldsymbol{r})\psi^{\dagger}(\boldsymbol{r}')v(\boldsymbol{r}-\boldsymbol{r}')\psi(\boldsymbol{r}')\psi(\boldsymbol{r})d\boldsymbol{r}d\boldsymbol{r}'. \quad (2)$$

Here $v(\boldsymbol{r})$ is the Coulomb interaction,

$$v(\boldsymbol{r}) = \frac{e^2}{4\pi\epsilon_0\varepsilon r}, \quad (3)$$

and $v_0(\boldsymbol{r})$ is the periodic potential energy due to the lattice structure, as modulated by any variations in chemical composition that, for example, create the quantum well; the spin-orbit interaction could be easily included, but has been not written here for simplicity. By performing the transformation

$$\psi(\boldsymbol{r},t) \mapsto \psi(\boldsymbol{r},t)e^{ie\boldsymbol{A}_{nom}(t)\cdot\boldsymbol{r}/\hbar},$$

and substituting $\boldsymbol{E}(t) = -\partial\boldsymbol{A}_{nom}/\partial t$, Eq. (2) is rendered in the form of length-gauge for the electromagnetic coupling,

$$\mathcal{H}(t) = \mathcal{H}_0 + \mathcal{H}_{ext}(t) + \int \psi^{\dagger}(\boldsymbol{r})\psi^{\dagger}(\boldsymbol{r}')v(\boldsymbol{r}-\boldsymbol{r}')\psi(\boldsymbol{r}')\psi(\boldsymbol{r})d\boldsymbol{r}d\boldsymbol{r}',$$

where

$$\mathcal{H}_0 = \frac{-\hbar^2}{2m}\int \psi^{\dagger}(\boldsymbol{r})\nabla^2\psi(\boldsymbol{r})d\boldsymbol{r} + \int v_0(\boldsymbol{r})\psi^{\dagger}(\boldsymbol{r})\psi(\boldsymbol{r})d\boldsymbol{r},$$

and

$$\mathcal{H}_{ext}(t) = -e\boldsymbol{E}(t)\cdot\int \psi^{\dagger}(\boldsymbol{r})\boldsymbol{r}\psi(\boldsymbol{r})d\boldsymbol{r}$$

describes the driving of by external electromagnetic field within the dipole approximation. The Hamiltonian $\mathcal{H}_0$ defines a static eigenvalue equation

$$\left[-\frac{\hbar^2}{2m}\nabla^2 + v_0(\boldsymbol{\rho},z)\right]\varphi(\boldsymbol{\rho},z) = E\varphi(\boldsymbol{\rho},z),$$

where $\boldsymbol{\rho}=(x,y)$ in which the potential possesses the property of two-dimensional periodicity in $\boldsymbol{\rho}$ and confinement in z. Thus the in-plane wave vector, which we denote by $\boldsymbol{k}=(k_x,k_y)$, remains a good quantum number. The discrete levels at each $\boldsymbol{k}$ include both the periodicity and the confinement effects (more physically, a set of bands for each transverse state of the well), and we label them with the symbol ζ. Thus the basis functions are

$$\langle \boldsymbol{r}|\zeta,\boldsymbol{k}\rangle = u_{\zeta}(\boldsymbol{k};\boldsymbol{\rho},z)e^{i\boldsymbol{k}\cdot\boldsymbol{\rho}}, \quad (4)$$

and we denote the corresponding energies by $\hbar\omega_{\zeta}(\boldsymbol{k})$, which allows us to expand the electron field operator as

$$\psi(\boldsymbol{\rho},z) = \sum_{\zeta}\int \frac{d\boldsymbol{k}}{4\pi^2}a_{\zeta}(\boldsymbol{k})u_{\zeta}(\boldsymbol{k};\boldsymbol{\rho},z)e^{i\boldsymbol{k}\cdot\boldsymbol{\rho}},$$

where the eigenfunctions $u_{\zeta}(\boldsymbol{k};\boldsymbol{\rho},z)$ are appropriately normalized.

Turning now to the coupling with the classical electromagnetic field that occurs through $\mathcal{H}_{ext}(t)$, we expand the coupling in the basis, Eq. (4), to find

$$\mathcal{H}_{ext}(t) = \sum_{\zeta\zeta'}\int \frac{d\boldsymbol{k}}{4\pi^2}\hbar\phi_{\zeta\zeta'}(\boldsymbol{k},t)a^{\dagger}_{\zeta}(\boldsymbol{k})a_{\zeta'}(\boldsymbol{k}). \quad (5)$$

Subtleties arise in the calculation of the matrix elements $\phi_{\zeta\zeta'}$ (Refs. 11–13) because the coordinate $\boldsymbol{r}$ does not satisfy the periodic boundary conditions that the functions $u_{\zeta}(\boldsymbol{k};\boldsymbol{\rho},z)e^{i\boldsymbol{k}\cdot\boldsymbol{\rho}}$ satisfy. But those matrix elements have been shown to be given by the interband dipole matrix elements, $\boldsymbol{\xi}_{\zeta\zeta'}(\boldsymbol{k})$,

$$\phi_{\zeta\zeta'}(\boldsymbol{k},t) = -\frac{e}{\hbar}\boldsymbol{E}(t)\cdot\boldsymbol{\xi}_{\zeta\zeta'}(\boldsymbol{k}),$$

for $\zeta\neq\zeta'$, and the intraband connections $\boldsymbol{\vartheta}_{\zeta\zeta}$ (Ref. 11)

$$\phi_{\zeta\zeta} = \frac{e}{\hbar}\boldsymbol{E}(t)\cdot(i\nabla_k - \boldsymbol{\vartheta}_{\zeta\zeta}).$$

Finally, the Coulomb interaction in the above basis takes the form

$$\mathcal{H}(t) - \mathcal{H}_{ext}(t) = \frac{\hbar}{2}\sum_{\zeta_1,\ldots,\zeta_4}\int\left(\prod_{j=1}^{4}\frac{d\boldsymbol{k}_j}{4\pi^2}\right)V_{\zeta_1\zeta_4\zeta_2\zeta_3}(\boldsymbol{k}_1,\boldsymbol{k}_4;\boldsymbol{k}_2,\boldsymbol{k}_3) \times a^{\dagger}_{\zeta_1}(\boldsymbol{k}_1)a^{\dagger}_{\zeta_4}(\boldsymbol{k}_4)a_{\zeta_2}(\boldsymbol{k}_2)a_{\zeta_3}(\boldsymbol{k}_3).$$

It is convenient to write the matrix elements of the Coulomb potential as

$$V_{\zeta_1\zeta_4\zeta_2\zeta_3}(\boldsymbol{k}_1,\boldsymbol{k}_4;\boldsymbol{k}_2,\boldsymbol{k}_3) = \frac{1}{\hbar}\int\frac{d\boldsymbol{q}}{4\pi^2}v(\boldsymbol{q})\sum_{\boldsymbol{l}\boldsymbol{l}'}\delta(\boldsymbol{k}_1-\boldsymbol{k}_3-\boldsymbol{q}-\boldsymbol{l}) \times\delta(\boldsymbol{k}_2-\boldsymbol{k}_4-\boldsymbol{q}-\boldsymbol{l}')F^{\boldsymbol{l}\boldsymbol{l}'}_{\zeta_1\zeta_4\zeta_2\zeta_3}(\boldsymbol{k}_1,\boldsymbol{k}_4;\boldsymbol{k}_2,\boldsymbol{k}_3), \quad (6)$$

where $v(q)$ is the two-dimensional Fourier transform of the Coulomb potential,

$$v(q) = \frac{e^2}{2\epsilon_0\varepsilon q}.$$

The vectors $\boldsymbol{l},\boldsymbol{l}'$ that are summed over are reciprocal lattice vectors of the two-dimensional (2D) lattice, and the matrix elements $F^{\boldsymbol{l}\boldsymbol{l}'}_{\zeta_1\zeta_4\zeta_2\zeta_3}(\boldsymbol{k}_1,\boldsymbol{k}_4;\boldsymbol{k}_2,\boldsymbol{k}_3)$ are given by the integral

$$F^{\boldsymbol{l}\boldsymbol{l}'}_{\zeta_1\zeta_4\zeta_2\zeta_3}(\boldsymbol{k}_1,\boldsymbol{k}_4;\boldsymbol{k}_2,\boldsymbol{k}_3) = \int dz\int dz' e^{-q|z-z'|}F^{\boldsymbol{l}}_{\zeta_1\zeta_3}(\boldsymbol{k}_1\boldsymbol{k}_3;z)F^{\boldsymbol{l}'}_{\zeta_4\zeta_2}(\boldsymbol{k}_4\boldsymbol{k}_2;z'), \quad (7)$$

$$F^{\boldsymbol{l}}_{\zeta\zeta'}(\boldsymbol{k}\boldsymbol{k}';z) = \int_{cell} d\boldsymbol{\rho} u^*_{\zeta}(\boldsymbol{k};\boldsymbol{\rho},z)e^{-i\boldsymbol{l}\cdot\boldsymbol{\rho}}u_{\zeta'}(\boldsymbol{k}';\boldsymbol{\rho},z). \quad (8)$$

In Eq. (6), the terms $\boldsymbol{l}\neq 0$ or $\boldsymbol{l}'\neq 0$ arise from the conservation of total crystal momentum, which is only within a reciprocal lattice vector. Only for $\boldsymbol{l}=0$ and $\boldsymbol{l}'=0$ do they behave in the form expected in free space. We refrain from imposing such restrictions here as they have no bearing on the subsequent analysis, except for additional rules in the diagrammatic method to be described at the end of the paper.

Collecting all of the above notation and approximations, the full Hamiltonian can now be specified as

$$\begin{aligned}\hbar^{-1}\mathcal{H}(t) &\equiv H + H_{ext}(t)\\ &= \sum_{\zeta}\int \frac{d\boldsymbol{k}}{4\pi^2}\omega_{\zeta}(\boldsymbol{k})a^{\dagger}_{\zeta}(\boldsymbol{k})a_{\zeta}(\boldsymbol{k})\\ &\quad + \frac{1}{2}\sum_{\zeta_1,\ldots,\zeta_4}\int\left(\prod_{j=1}^{4}\frac{d\boldsymbol{k}_j}{4\pi^2}\right)V_{\zeta_1\zeta_4\zeta_2\zeta_3}(\boldsymbol{k}_1,\boldsymbol{k}_4;\boldsymbol{k}_2,\boldsymbol{k}_3)\\ &\quad \times a^{\dagger}_{\zeta_1}(\boldsymbol{k}_1)a^{\dagger}_{\zeta_4}(\boldsymbol{k}_4)a_{\zeta_2}(\boldsymbol{k}_2)a_{\zeta_3}(\boldsymbol{k}_3)\\ &\quad + \sum_{\zeta\zeta'}\int\frac{d\boldsymbol{k}}{4\pi^2}\phi_{\zeta\zeta'}(\boldsymbol{k},t)a^{\dagger}_{\zeta}(\boldsymbol{k})a_{\zeta'}(\boldsymbol{k}). \quad (9)\end{aligned}$$

Although the contribution of phonons could be easily added, it is not included at this stage to avoid unnecessary complications in the formalism. Even without it we can address situations with intermediate carrier densities at low temperature, where the Coulomb interaction is the dominant decoherence mechanism.

B. Green functions

If there are multiple quantum wells in the sample, we follow the strategy of Appendix A to take into account their interactions. For each quantum well, we calculate the charge and current densities, $\langle\bar{\rho}(\boldsymbol{r},t)\rangle$ and $\langle\bar{\boldsymbol{J}}(\boldsymbol{r},t)\rangle$, respectively, as functionals of the field $\boldsymbol{E}(t)$ appearing in Eq. (5) using the method of Green functions. The single-particle Green function is defined as

$$G(12) = -i\langle\mathcal{T}_C a(1)a^{\dagger}(2)\rangle. \quad (10)$$

Here, and in the following discussion, we follow the standard practice of using numbers to denote a set of arguments not shown explicitly; thus $1=(\boldsymbol{k}_1,t_1,\zeta_1)$ where t_1 is time variable on the Keldysh contour. If we perform a transformation from the basis function to real space, then analogously $1=(\boldsymbol{r}_1,t_1)$. To denote equal time limits, we define the symbol $1^+=(\boldsymbol{k}_{1^+},t_1^+,\zeta_{1^+})$, where t_1^+ stands for infinitesimal advancement of time variable *on the Keldysh contour*. The symbol $\mathcal{T}_C$ orders the operators on the contour, and the meaning of $\langle O\rangle$ for an arbitrary operator, O, is through a trace with a statistical operator $\hat{\rho}$ (not to be confused with the single-particle density matrix),

$$\langle O\rangle = \frac{1}{Z_C}\mathrm{Tr}[O\hat{\rho}e^{-iS[\Phi]}]. \quad (11)$$

The factor Z_C is the general generating functional

$$Z_C[\Phi] = \mathrm{Tr}[\mathcal{T}_C\hat{\rho}e^{-iS[\Phi]}], \quad (12)$$

and

$$S[\Phi] = \int_C d\tau\int d\boldsymbol{r}H[a^{\dagger},a] + \int_C \Phi(12)a^{\dagger}(1)a(2) \quad (13)$$

is defined for an arbitrary bilinear coupling via the *bare* two-time external potential $\Phi(12)$. In the physical limit, $\Phi(12)$ will depend on a single time and is identified with $\phi_{\zeta\zeta'}(\boldsymbol{k},t)$ of Eq. (5) above, as discussed in Sec. IV. From the definitions of the charge and current densities, we see that

$$\langle\bar{\rho}(\boldsymbol{r},t)\rangle = -ieG(\boldsymbol{r}t;\boldsymbol{r}t^+), \quad (14)$$

$$\langle\bar{\boldsymbol{J}}(\boldsymbol{r},t)\rangle = -\frac{e\hbar}{2m}\lim_{\boldsymbol{r}\to\boldsymbol{r}'}[\nabla_{\boldsymbol{r}}G(\boldsymbol{r}t;\boldsymbol{r}'t^+) - \nabla_{\boldsymbol{r}'}G(\boldsymbol{r}t;\boldsymbol{r}'t^+)]. \quad (15)$$

Thus the self-consistent calculation determines $G(12)$ via the Hamiltonian (9). To finally determine the signal in a TDFS experiment, the quantities $\langle\bar{\rho}_{eff}(\boldsymbol{r},t)\rangle$ and $\langle\bar{\boldsymbol{J}}_{eff}(\boldsymbol{r},t)\rangle$ of Eq. (A9) are then calculated (see Appendix A), and treated as the source of the signal. The rest of the paper is devoted to developing the formal machinery to determine $G(12)$ in the presence of many-body interactions.

Prior to the introduction of the pulse sequences we assume that the system is in a quasiequilibrium state that evolves on a time scale much longer than the one associated with the optical excitation; any photoluminescence that would appear is neglected. The Green function G_{Q} associated with this state leads to vanishing signal at the respective frequencies. We handle the subsequent optical excitation by writing the full Green function as

$$G(12) = G_{\mathrm{Q}}(12) + \Delta G(12), \quad (16)$$

where $\Delta G(12)$ describes the effects of optical excitation, and will lead to nonvanishing $\langle\bar{\boldsymbol{J}}(\boldsymbol{r},t)\rangle$, and hence to a signal field. While the defining Eq. (10) introduces $G(12)$ as a functional of the driving field Φ, $G(12)=G(12;\Phi)$, it is convenient to introduce a self-consistent field $U_{Hartree}$,

$$U_{Hartree}(1,2) = \Phi(12) - i\int V(13;42)G(43), \quad (17)$$

that represents the dressing of the external driving field by the medium of charges interacting via the bare Coulomb interaction. Here the Coulomb interaction has also been rewritten with implied delta functions in time,

$$V(14;23) = V_{\zeta_1\zeta_4\zeta_2\zeta_3}(\boldsymbol{k}_1,\boldsymbol{k}_4;\boldsymbol{k}_2,\boldsymbol{k}_3)\delta(t_1-t_3^+)\delta(t_2^+-t_4)\delta(t_1-t_2), \quad (18)$$

to establish a uniform notation with four-point effective interactions below. The change in this self-consistent field due to the pulses of light is given by

$$U(12) \equiv U_{Hartree}(12) - U_{\mathrm{Q}}(12), \quad (19)$$

where the self-consistent field in the (quasi-)equilibrium states is just

$$U_{\mathrm{Q}}(12) = -i\int V(13;42)G_{\mathrm{Q}}(43). \tag{20}$$

The Dyson equation the Green function satisfies can then be written in the form

$$G(12) = G_0(12) + G_0(11')U_{\mathrm{Q}}(1'1'')G(1''2) + G_0(11')U(1'1'')G(1''2) + G_0(11')\Sigma(1'1'')G(1''2), \tag{21}$$

introducing a self-energy $\Sigma(1'1'')$. With this equation in hand, the strategy now is to treat the basic field U as the *effective field*, such that $\Phi=\Phi[U]$. Therefore when written as a solution to Eq. (21), G is functionally dependent on U rather than on Φ, or in other words $G(12;U)=G(12;\Phi[U])$. Similarly the self-energy is also taken as a functional of U.

Increasing the effective field from $U(34)$ to $U(34)+\delta U(34)$ leads to a change in the Green function from $G(12)$ to $G(12)+\delta G(12)$, where for infinitesimally small $\delta U(34)$ we have $\delta G(12)=P(14;23)\delta U(34)$, and the functional derivative

$$P(14;23) \equiv \frac{\delta G(12)}{\delta U(34)} \tag{22}$$

is evaluated at $U(34)$. Hence in the limit of a weak effective field we have

$$\Delta G(12) = \left[\frac{\delta G(12)}{\delta U(34)}\right]_{\mathrm{Q}} U(34) + \left[\frac{\delta^2 G(12)}{\delta U(34)\delta U(56)}\right]_{\mathrm{Q}} U(34)U(56) + \left[\frac{\delta^3 G(12)}{\delta U(34)\delta U(56)\delta U(78)}\right]_{\mathrm{Q}} U(34)U(56)U(78) + \cdots = P(14;23)U(34), \tag{23}$$

where the subscript Q indicates that the functional derivative is evaluated in the quasiequilibrium state, with $U=0$, and we have written

$$P(14;23) = \left[\frac{\delta G(12)}{\delta U(34)}\right]_{\mathrm{Q}} + \left[\frac{\delta^2 G(12)}{\delta U(34)\delta U(56)}\right]_{\mathrm{Q}} U(56) + \left[\frac{\delta^3 G(12)}{\delta U(34)\delta U(56)\delta U(78)}\right]_{\mathrm{Q}} U(56)U(78) + \cdots. \tag{24}$$

Despite the fact that one then has to extract an expression for ΔG in terms of Φ, the driving field, at the end of the calculation, we will see that this approach simplifies the analysis.

Since the use of the expansion (23) for $\Delta G(12)$ in the expressions (14) and (15) leads to expansions for $\langle\bar{\rho}(\boldsymbol{r},t)\rangle$ and $\langle\bar{\boldsymbol{J}}(\boldsymbol{r},t)\rangle$, ultimately in powers of the driving field, that expansion constitutes the Green function form of the usual expansion in nonlinear optics of the response of the system in increasing powers of the electric field. In a TDFS experiment the signal in the background-free direction will be from the third term in Eq. (24) when it is used in Eq. (23). All three incident pulses will contribute to all the $U(ij)$ and P, of course, but the signals due to the different combinations of the pulses will propagate in different directions. For example, one contribution to the signal will result from each of the $U(34)$, $U(56)$, and $U(78)$ corresponding to a different pulse, and it will propagate in the four-wave mixing direction. Thus in general a contribution to the signal can be identified as the nonequilibrium response to a probe of a system excited by pump pulses. The full signal is a sum over all 27 possibilities labeling the three pulses as probe or pump pulses.

In doped semiconductors, the quasiequilibrium state may consist of interacting electrons, in equilibrium with the lattice. This is a true equilibrium situation, where the response of the system depends only on differences in time. In terms of Wigner variables, $\tau=t_1-t_2$, and $t=(t_1+t_2)/2$, G_{Q} depends only on τ. We may also allow greater flexibility by considering an unexcited semiconductor that is excited optically to produce a nonthermal distribution of carriers. In this scenario $G_{\mathrm{Q}}(t,\tau)$ depends on t, and this dependence is slowly varying with respect to the dynamics induced by the subsequent TDFS excitation. This more complex scenario can be handled by a multiple-scale expansion in the variable t.

C. Effective two-particleinteraction

Central to this approach are the properties of $P(14;23)$, which we identify here. For the derivation of the integral equations that arise, we refer to the reader to one of a number of standard references on Green function theory.[6,10,14–19] The quantity $P(14;23)$ satisfies the Bethe-Saltpeter equation (BSE),

$$P(14;23) = G(13)G(42) + \int G(11')G(2'2)I^{(2)}(1'6;2'5)P(54;63), \tag{25}$$

where the *effective two-particle interaction*,

$$I^{(2)}(1'6;2'5) = \frac{\delta\Sigma(1'2')}{\delta G(56)}. \tag{26}$$

Using the diagrammatic notation indicated in Fig. 1, the BSE equation is sketched in Fig. 2. Since $I^{(2)}$ is one of the basic objects that will be used in the rest of the paper, we briefly discuss it here using the diagrams shown in Fig. 3; in Appendix B we work out the detailed algebraic form that is captured by those diagrams.

The first diagram indicates the basic interaction between electrons in interparticle scattering, and corresponds to an effective Coulomb interaction $W(14;23)$ with a vertex correction $\Gamma(14;23)$. The effective interaction is defined as the solution of the integral equation

$$W(14;23) = V(14;23) - i\int V(15;63)P(66';55')W(5'4;26'). \tag{27}$$

In its diagrammatic form, the incoming and outgoing lines are attached to W as shown in Fig. 1. The vertex correction

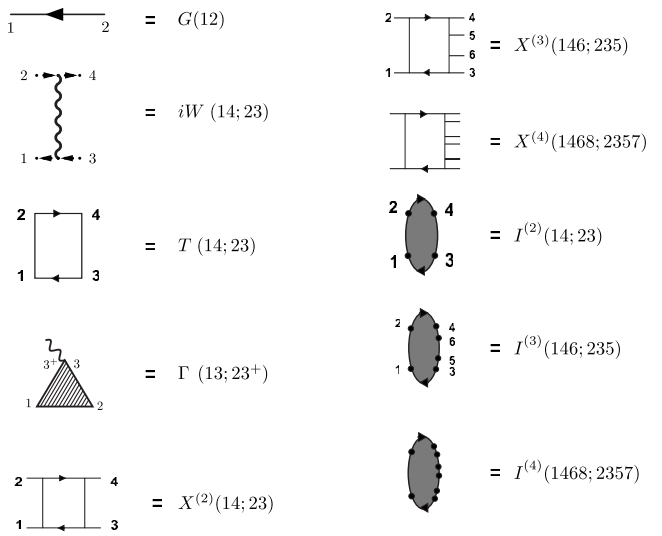

FIG. 1. Graphical symbols for constructing diagrams. Note that $P(14;23)=X^{(2)}(14;23)$.

corrects $P(14;23)$ from its simplest approximation,

$$P^{(0)}(14;23) = G(13)G(42), \tag{28}$$

such that the exact $P(14;23)=G(11')G(2'2)\Gamma(1'4;2'3)$, and

$$\Gamma(14;23) = -\frac{\delta G^{-1}(12)}{\delta U(34)} = \delta(13)\delta(24) + T(12';21')G(1'3)G(42'), \tag{29}$$

where we have introduced a T-matrix as the solution of the integral equation

$$T(14;23) = I^{(2)}(14;23) + I^{(2)}(12';21')G(1'5)G(62')T(54;63), \tag{30}$$

The second and third diagrams of Fig. 3 play a crucial role in the decoherence process that occurs due to the scattering of an electron from a correlated pair, and we will turn to them in Sec. III C. The fourth and fifth arise entirely from $\delta W/\delta G$, and are a precursor for a new scattering channel. Insight into their nature follows from using an expression for the self-energy in terms of the T-matrix (or Γ), that avoids explicit reference to the inverse Green function. From the definition (21) of the self-energy, and those of the vertex correction (29) and T-matrix (30), we find

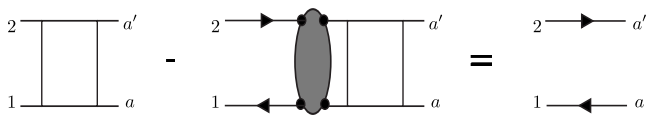

FIG. 2. The BSE for four-point function.

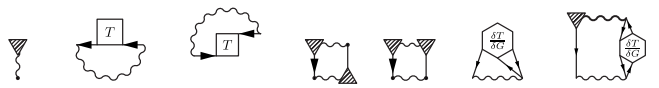

FIG. 3. Diagrams for $I^{(2)}$.

$$\Sigma(12) = i\int W(13;3'1')G(1'1'')\Gamma(1''3';23) = i\int W(13;21')G(1'3) + i\int W(13;3'1')G(1'1'')T(1''2'';23'')G(3''3)G(3'2''). \tag{31}$$

Iterating the coupled Eqs. (26), (30), and (31) it becomes evident that this new channel involves a "horizontal" ladder series in the self-energy and represents repeated interaction of the single particle with another particle in the system. By crossing symmetry[15,17] in the exact formulation, this channel can simply be represented by the same equation as Eq. (30) but with the effective interaction now acting on 1,3 in $T(14;23)$. While optical excitation creates coherence only between the ground state and an excited state, correlations such as those underlying dynamical interactions transfer this coherence to coherence between excited states. As shown in II, the fourth and fifth diagrams in Fig. 3 are the kind that describe one such transfer mechanism. The coherences thus generated, sometimes referred to as Raman coherences,[20] decay mainly under the influence of the first three diagrams. However, the fourth and fifth diagrams also make further contributions to the dynamics when there is an electron-hole plasma at reasonably high density regimes, but below the Mott transition point such that bound electron-hole states still exist. In this case, they significantly affect the nature of two-particle interaction.

Finally, the last two diagrams arise from the six-point function formed by the variational derivative of the T-matrix itself. The six-point function is reducible, and therefore generates diagrams in Fig. 3 that are combinations of the two- and four-point functions. In particular, note that the set of diagrams is asymmetric in the sense that diagrams that would be obtained by flipping them upside down are not shown explicitly. These diagrams do occur, and are contributed precisely by these last two terms. In an exact formulation these are guaranteed to occur due to the equivalence of the two self-energy formulas,

$$\Sigma(11')G(1'2) = iW(13;3'^{+}1')P(1'3'^{+}), \tag{32}$$

$$G(11')\Sigma(1'2) = iP(13';2'^{+})W(2'3;3'^{+}2). \tag{33}$$

Their equality implies that the particle number, and energy are conserved, which is an important property to build into approximations. Therefore in an approximate treatment, which in general picks a finite number of vertex diagrams, the symmetric diagrams can be included "by hand" and excluded from any approximations for the six-point function. This corresponds to including all diagrams of the same to-

pology (i.e., those which differ only by relabeling external vertices). The remaining contribution of $\delta T/\delta G$ is then to used generate scattering channels of topologies beyond those already included in the (approximate) T-matrix being differentiated.

In general, the vertex correction contains *all* two-particle reducible graphs, and represents an infinite number of scattering channels. However, in a given regime of density, temperature, and optical frequencies, only a few will generally be dominant. Thus any approximation would necessarily pick a particular analytical form for $\Gamma[W,G,P,\ldots]$ as a starting point of the self-consistent calculation. We now turn to ours.

III. RESPONSE FUNCTIONS FRAMEWORK

A. Susceptibility expansion

Returning to the expression (16) for $G(12)$ and the expansion (23) for its deviation $\Delta G(12)$ from quasiequilibrium, we can write

$$\Delta G(12) = \Delta G_1 + \Delta G_2 + \Delta G_3 + \cdots = X^{(1)}(12) - X_{\mathrm{Q}}^{(1)}(12). \tag{34}$$

In anticipation of some future notation $G(12)$ and $G_{\mathrm{Q}}(12)$ are written as $X^{(1)}(12)$ and $X_{\mathrm{Q}}^{(1)}(12)$ respectively. For any function, O, we define

$$\Delta O_n = \int \left(\frac{\delta^n O}{\delta U(1''1')\delta U(2''2')\cdots\delta U(n''n')} \right)_{\mathrm{Q}} \times U(1''1')U(2''2')\cdots U(n''n'). \tag{35}$$

The quantities ΔG_n are of fundamental interest in predicting experimental results. Since they are also central to the formalism, we use a separate symbol for them,

$$\mathfrak{X}_n^{(1)}(12) \equiv \Delta G_n(12). \tag{36}$$

The meaning of the superscript will become clear below. In the absence of Coulomb interactions, from Eq. (25) we see that $P(14;23)=G(13)G(24)$, and constructing the expressions for the $\mathfrak{X}_{1\ldots3}^{(1)}(12)$ leads to

$$\mathfrak{X}_1^{(1)}(12) = G_{\mathrm{Q}}(13)U(34)G_{\mathrm{Q}}(42), \tag{37}$$

$$\mathfrak{X}_2^{(1)}(12) = G_{\mathrm{Q}}(13)U(34)\mathfrak{X}_1^{(1)}(42) + \mathfrak{X}_1^{(1)}(13)U(34)G_{\mathrm{Q}}(42), \tag{38}$$

$$\mathfrak{X}_3^{(1)}(12) = \mathfrak{X}_1^{(1)}(13)U(34)\mathfrak{X}_1^{(1)}(42) + G_{\mathrm{Q}}(13)U(34)\mathfrak{X}_2^{(1)}(42) + \mathfrak{X}_2^{(1)}(13)U(34)G_{\mathrm{Q}}(42). \tag{39}$$

That is, the set of three dynamical variables $\{\mathfrak{X}_1^{(1)},\mathfrak{X}_2^{(1)},\mathfrak{X}_3^{(1)}\}$ is closed and this system of equations fully captures the dynamics of this noninteracting system. In this limit, the coherence between the ground state and a particle-hole pair is preserved and uniquely determines all higher order correlations. This is not true when Coulomb interactions are present, which can build nontrivial correlations among the particles. Then the equations for the variables $\mathfrak{X}_n^{(1)}$ involve quantities $\mathfrak{X}_n^{(2)}(14;23)$ that become dynamical variables themselves, where in general for $j>1$ we put

$$\begin{aligned}\mathfrak{X}_n^{(j)}(1a_1'\ldots a_{j-1}';2a_1\ldots a_{j-1}) &\equiv \Delta X_n^{(j)}(1a_1'\ldots a_{j-1}';2a_1\ldots a_{j-1}) \\ &= \int \left(\frac{\delta^n X^{(j)}(1a_1'\ldots a_{j-1}';2a_1\ldots a_{j-1})}{\delta U(1''1')\ldots\delta U(n''n')} \right)_{\mathrm{Q}} \times U(1''1')\cdots U(n''n') \\ &= \int X_{\mathrm{Q}}^{(j+n)} U(1''1')\cdots U(n''n'),\end{aligned} \tag{40}$$

and where for $j>0$ it is useful to define $X^{(j+1)}$ and $X_{\mathrm{Q}}^{(j+1)}$ as, respectively, the $2j$-point correlation functions

$$X^{(j+1)}(1a_1'\ldots a_j';2a_1\ldots a_j) \equiv \frac{\delta^j G(12)}{\delta U(a_1a_1')\cdots\delta U(a_ja_j')}, \tag{41}$$

evaluated at $U\neq 0$, and their values at $U=0$ as

$$X_{\mathrm{Q}}^{(j+1)}(1a_1'\ldots a_j';2a_1\ldots a_j) \equiv \left[\frac{\delta^j G(12)}{\delta U(a_1a_1')\cdots\delta U(a_ja_j')} \right]_{\mathrm{Q}}. \tag{42}$$

Again, since $\Delta X_n^{(j)}$ are central to the formalism, we use a separate symbol, $\mathfrak{X}_n^{(j)}$, for them. Thus $\mathfrak{X}_n^{(j)}$ is generally the contribution to order $\mathcal{O}(U^n)$ of the deviation $X^{(j)}-X_{\mathrm{Q}}^{(j)}$ of order $\mathcal{O}(U^n)$, and

$$X^{(j)} - X_{\mathrm{Q}}^{(j)} \equiv \Delta X^{(j)} = \sum_n \mathfrak{X}_n^{(j)}, \tag{43}$$

of which Eq. (34) is the special case for $j=1$.

In the presence of Coulomb interactions the $\mathfrak{X}_n^{(2)}$ can no longer be written in terms of the variables $\{\mathfrak{X}_1^{(1)},\mathfrak{X}_2^{(1)},\mathfrak{X}_3^{(1)}\}$, and they acquire a dynamics beyond that implied by simple factorization (28) of $P(14;32)$ as a product of Green functions. The BSE and the discussion of $I^{(2)}$ above implies that the $\mathfrak{X}_n^{(2)}$ are coupled to the $\mathfrak{X}_n^{(3)}$, and so on. Thus, in the presence of interactions, the set of dynamical variables expands to include $\mathfrak{X}_n^{(j)}$ for all $j=1,\ldots\infty$.

At first sight it might seem better to work directly with the $X^{(j)}$, since what is required for comparison with experiment is simply $X_{\mathrm{Q}}^{(4)}$ [see Eqs. (24), (35), and (43)]. The equations for $X^{(j)}$ consist of the products of $X^{(j')}$ for $j'<j$, and an interaction of the same order, j, which builds nontrivial correlations and couples them to $X^{(k)}$ for $k>j$. The factorization follows from the lengthy but straightforward integral equations derived in Appendix C for up to $j=4$, and shown diagrammatically in Fig. 4. In these diagrams, the effective interactions $I^{(n)}$ are defined as

$$I^{(n)}(12'\ldots n';1'2\ldots n) = \frac{\delta^{n-1}\Sigma(11')}{\delta G(22')\cdots\delta G(nn')}, \quad n>1. \tag{44}$$

of which the $I^{(2)}$ defined earlier Eq. (26) is a special case. The equations for the six ($j=3$) and eight ($j=4$) point correlation functions have a simple combinatorial structure, in

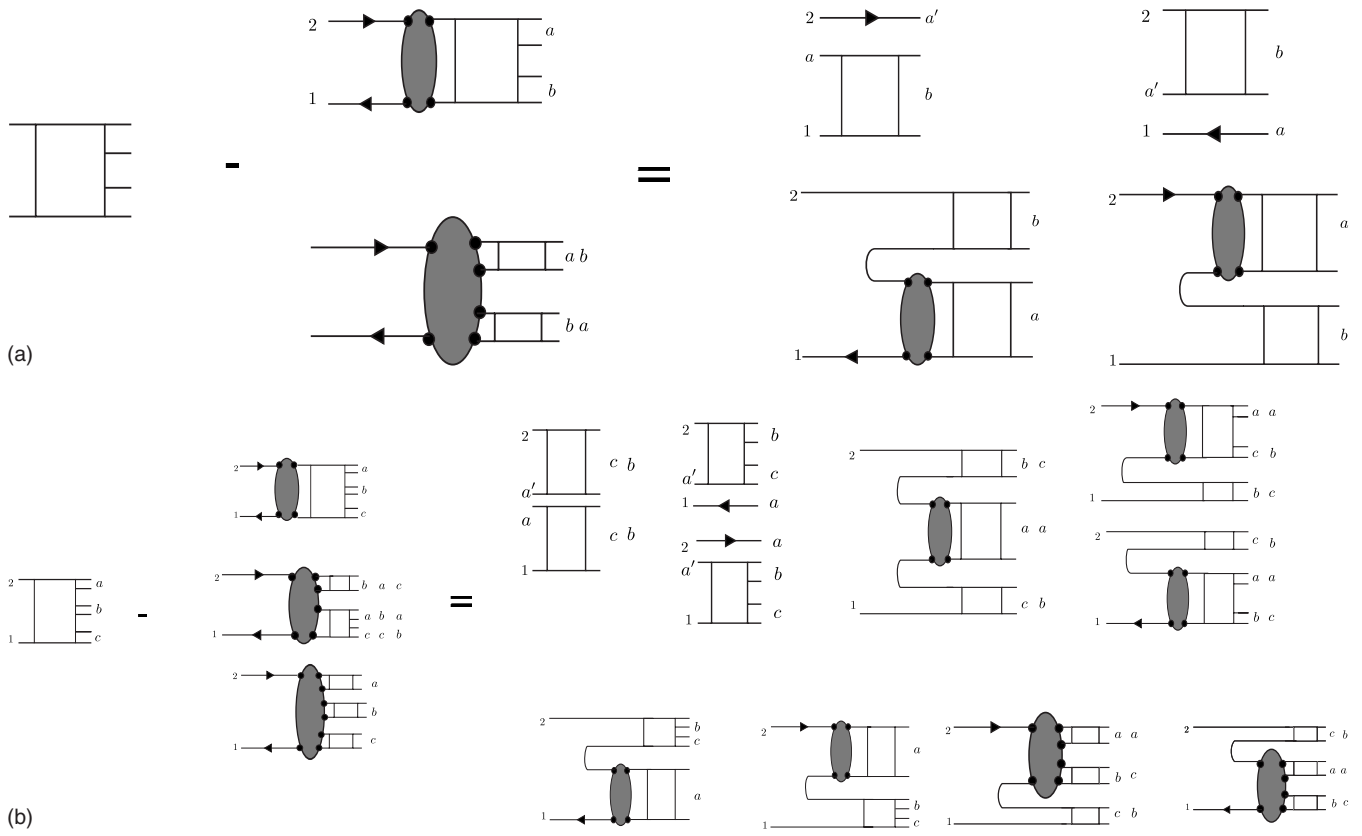

FIG. 4. The BSE's for six- ($X^{(3)}$) and eight-point ($X^{(4)}$) functions. All permutations are shown explicitly. We use a to represent the set (a,a') etc.

which the correlation function is factorized into all possible combinations of the lower order correlation functions (Fig. 4). Diagrams separated into unconnected components represent the independent evolution of these components. In some of the diagrams, these components are brought into interaction either by a 4, 6, or 8 point effective interaction $I^{(2)}$, $I^{(3)}$, or $I^{(4)}$. They arise out of Coulomb interaction, and thus form an essential part of the many-body physics.

The exact solution of these integral equations yields $X_{\mathrm{Q}}^{(4)}$, from which ΔG can be obtained by integration. However, such a calculation is prohibitive as it includes immensely complex nonperturbative effects arising from the summation of infinite subsets of diagrams. So we abandon this approach in favor of focusing on the $\mathfrak{X}_n^{(j)}$, which provide the essential information for comparison with experiment in an alternative fashion. As we show below in Sec. III C, and in a following paper, it is possible to derive differential equations for the $\mathfrak{X}_n^{(j)}$ at a chosen level of approximation. Analytically, these equations of motion (EOM) offer insight by explicitly identifying the rates of different processes. Numerically, the self-consistent solution of these equations, via time stepping, allows many nonperturbative effects to be included automatically. The formulation of the problem is reduced to a dynamical interplay of the deviations $\mathfrak{X}_n^{(j)}$ [see Eq. (43)], where the rules of the dynamics are specified in the interactions that depend on the quasiequilibrium correlation functions.

We devote the following sections of the paper to these equations of motion.

B. Hierarchy of correlation functions and its approximate termination

A first step is the description of the hierarchy coupling the $\mathfrak{X}_n^{(1)}$ of interest Eq. (34) to the $\mathfrak{X}_n^{(2)}$, and the $\mathfrak{X}_n^{(2)}$ to the $\mathfrak{X}_n^{(3)}$, and so on; the identification of approximations that can be made to truncate the hierarchy; and description of the consequences of this truncation on the properties of the correlation functions being studied here. That is the goal of this section.

To discuss the hierarchy economically, it is convenient to extend the definition (30) of $T(14;23)$ to terms involving higher order derivatives,

$$T^{(n)}(12'\ldots n';1'2\ldots n) = \frac{\delta^{n-2}T(11')}{\delta U(22')\ldots\delta U(nn')}, \quad n \geq 2. \tag{45}$$

With this term in hand we will be able to identify the nonfactorizable parts of correlation functions. To illustrate this we use a schematic notation in which we suppress the arguments of the functions, and discuss the contribution $T^{(n)}$ makes to $X^{(n)}$. For $n=2$, the function $T^{(2)}$ corresponds to the one-particle irreducible amputated diagrams[17–19] comprising $X^{(2)}$, i.e.,

$$GGT^{(2)}GG = X^{(2)} - GG.$$

Relationships of this type are explained in Appendix D. Differentiating with respect to U, we obtain

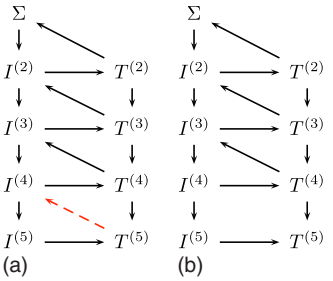

FIG. 5. (Color online) Hierarchy of $I^{(n)}$ and $T^{(n)}$ in exact form (top left) and cut at eight-point level (top right). The arrows point to the function that needs as input the function at its tail. The dashed arrow is the link that is broken in terminating the hierarchy.

$$GGT^{(3)}GG = X^{(3)} - 2X^{(2)}G - 4X^{(2)}GGGT^{(2)},$$

where the numerical factors indicate the number of terms of the same topology. The second term on the right-hand side is unconnected, involving independent propagation of single- and two-particle correlation functions. The third term is single-particle reducible since only one leg of $X^{(2)}$ is connected to $T^{(2)}$. From the graphical six-point BSE (Fig. 4) it is clear that $X^{(3)}$ is a sum of these two terms and single-particle irreducible terms. Therefore $T^{(3)}$ must equal single-particle irreducible contributions to $X^{(3)}$ with four legs amputated. Similarly, $T^{(4)}$ consists of analogous diagrams for $X^{(4)}$ and so on. Expressing the correlation functions using $T^{(n)}$ has the advantage that the trivial effects of independent propagation, which are strictly determined by lower order correlation functions already at a given particle order, are removed. Thus these functionals bring in the fully interacting components at each order j.

Through the dependence (31) of the self-energy on $T^{(2)}$, the functional $I^{(2)}$ contains a contribution from the variational derivative of $T^{(2)}$ via Eq. (44), and this derivative is related to $T^{(3)}$ via Eq. (45). This particular term is the sum of two contributions that can be represented schematically by the following diagrams:

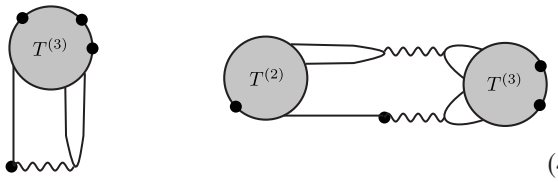

(46)

where the dots represent external vertices, and the solid circles represent the $T^{(n)}$ as indicated. The number of lines and dots on the shaded circles equals the number of arguments for the corresponding $T^{(n)}$, and therefore identify its superscript n. These two contributions to $I^{(2)}$ both contain the functional $T^{(3)}$. When these diagrams are differentiated again to obtain $I^{(3)}$, they will bring in a contribution of $T^{(4)}$, and thus the hierarchy shown in Fig. 5 ensues. Since $T^{(n)}$ is related to $X^{(n)}$ by n incoming and outgoing quasiparticles, the effective interaction $I^{(n)}$ can be viewed as becoming dependent on $X^{(n+1)}$. This effective interaction in the equation for $X^{(n)}$ couples it to $X^{(n+1)}$ and results in a parallel hierarchy for $X^{(n)}$; the explicit conversion between $T^{(n)}$ and $X^{(n)}$ is shown in Appendix D up to $n=4$.

The exact solution has the property that the self-energy, Σ, is consistent with *all* $T^{(n)}$, which requires summation of *all* scattering channels. This means, in particular, that if the functional derivative of Σ with respect to G is substituted in the Eq. (30) for $T^{(2)}$, then its solution is self-consistent with the $T^{(2)}$ matrix that Σ explicitly depends on via Eq. (31). The hierarchy necessitates that this hold not just for $T^{(2)}$, but also for $T^{(n)}$ on which the self-energy depends implicitly. Anything short of this, and therefore any practical iterative method of calculation, will break this consistency.[21,22]

It is instructive to consider how the consistency is broken in the well-known Kadanoff-Baym approach.[14,16] As an example, consider the T-matrix for the Bethe-Goldstone equation,[16] which is an example of a conserving approximation,

$$T^{(2)}_{approx} = V + VGGT^{(2)}_{approx}. \tag{47}$$

The approximate Σ is written as $\Sigma_{approx} = T^{(2)}_{approx}G$. The latter is then differentiated to obtain an algebraic expression,

$$I^{(2)}_{approx} = T^{(2)}_{approx} + \frac{\delta T^{(2)}_{approx}}{\delta G}G, \tag{48}$$

which when substituted in the BSE provides a two-particle correlation function that obeys conservation laws. However, the functional $I^{(2)}_{approx}$ is clearly not equal to the kernel, V, in Eq. (47), and therefore the complete set of single and two particle equations is not self-consistent. It also means that when $I^{(2)}_{approx}$ is used in the BSE, $P_{approx}(14;23)$ contains scattering in only two pairs of coordinates, namely 12 and 34. Nonetheless, the diagrams that contribute to Σ_{approx} ensure that it is still a functional derivative of some functional, and this is a sufficient condition for macroscopic conservation to hold.

In view of the underlying lattice, we do not expect momentum conservation to hold in solids. The particle number conservation for G, and the conservation of the total energy, requires only that the approximate $T^{(2)}$ obey $T^{(2)}(14;23) = T^{(2)}(41;32)$, which can be easily guaranteed by symmetrizing the integral equation for $T^{(2)}$. These are conditions (A) and (B) of the classic Kadanoff-Baym paper,[16] and if P is generated from such a G via functional differentiation (22), then it inherits these conservation laws from G. These translate into sum rules for conductivities and other quantities that describe linear response. On the other hand, including scattering between all pairs of external vertices of the correlation functions, as opposed to just two for P_{approx}, has important consequences for the decoherence of many-body states (see also II). We therefore follow the latter route below, and will see that it means losing the ability to make a general statement about sum rules for two, and higher particle correlations.

To proceed we will restrict ourselves to perturbative expansion in the field up to order 3, i.e., three pulse experiments. In the exact eight-point equation, Fig. 4(b), the effective interaction $I^{(4)}$ will depend on $T^{(5)}$ via the diagram,

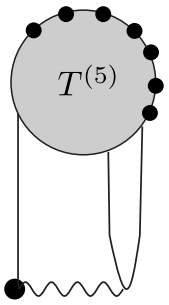

(49)

This diagram is at most contracted with three field-dressed correlation functions, and when they are all placed on the $T^{(5)}$, there remains one vertex exposed on it, which together with the vertex at the bottom right corner gives a two-point function that contributes to the self-energy of third order in the field. It is clear from this diagram that at least one pair of the external vertices of $T^{(5)}$ is already closed on itself, and connected to the rest of the self-energy diagram by an interaction line. The closure and the accompanying contraction with the field generates a field-dressed functional, $\Delta T_k^{(5-k)}$, which describes the k^{th} order deviation of $T^{(5-k)}$ from its quasiequilibrium value. To convince oneself that this is correct, one need only write the self-energy expression (suppressing the arguments) as, $\Sigma = WG + WGGGT$, [cf. Eq. (31)] and then expand each side of the equation to third order in field by expanding each quantity as in Eq. (34). Then one sees that the contribution $[WGGG]_{\mathrm{Q}}\Delta T_3^{(2)}$ in this expansion, and the expression corresponding to placing all three field lines on $T^{(5)}$ in the above diagram, have the same form. Thus we identify the $T^{(5)}$ connected to three field lines with $\Delta T_3^{(2)}$, and in general we identify $\Delta T_k^{(n-k)}$ with a kth order field-induced deviation in $T^{(n)}$. Examining the diagrammatic equations in Fig. 4, and the Dyson equation, we see that they depend explicitly only on the *field-dressed* functionals $\Delta T_1^{(2\ldots4)}$, $\Delta T_2^{(2\ldots3)}$, and $\Delta T_3^{(2)}$, and the quasiequilibrium functional $T_Q^{(2)}$. Equivalently we can state this dependence in terms of the effective interaction $I_Q^{(2)}$, and the field-induced deviations in it, $\Delta I_1^{(2\ldots4)}$, $\Delta I_2^{(2\ldots3)}$, and $\Delta I_3^{(2)}$.

From the above analysis, we see that each term in each of the BSE's [Figs. 4(a) and 4(b)] can be written as a product of $\mathfrak{X}_n^{(j)}$ and $\Delta I_n^{(j)}$, or the field-induced deviations in the correlation functions and effective interactions, respectively. The resulting equations are still exact to all orders in Coulomb interaction so long as exact expression for $\Delta I_n^{(j)}$ is known. In general such an expression would be dependent upon all $\mathfrak{X}_n^{(j)}$, and would not be possible to specify in practice. Therefore, at this point, we introduce an approximation strategy, or *phenomenology*, into the formalism by demanding that a model for $I^{(2)}$, $I^{(3)}$, and $I^{(4)}$ be specified in a way that these functionals are written as functions of the correlations $X^{(1\ldots3)}$ and W. Note that none of these quantities has been forced to be at quasiequilibrium. We thus have

$$I^{(j)} = I^{(j)}(W, X^{(1)}, X^{(2)}, X^{(3)}). \tag{50}$$

The arguments of the function $I^{(j)}$ correspond to subgraphs consisting of a possibly infinite number of diagrams constructed out of G and W in the exact $I^{(j)}$. We treat these subgraphs as independent objects in the model $I^{(j)}$. To write the (model) field-induced deviations $\Delta I_n^{(j)}$, we need the field-induced deviations in the screened interaction, W. Using Eq. (27), it can be written in terms of $X^{(j)}$, and W via

$$\frac{\delta W}{\delta U} = W\frac{\delta X^{(2)}}{\delta U}W = WX^{(3)}W. \tag{51}$$

We let

$$\Delta W_n(14;23) = \frac{\delta^n W(14;23)}{\delta U(\bar{1}\bar{1}') \ldots \delta U(\bar{n}\bar{n}')} U(\bar{1}\bar{1}') \ldots U(\bar{n}\bar{n}'), \tag{52}$$

which allows us to write $\Delta I_n^{(j)}$ as follows:

$$\Delta I_1^{(j)} = \left(\frac{\partial I^{(j)}}{\partial W}\right)_{\mathrm{Q}} \Delta W_1 + \left(\frac{\partial I^{(j)}}{\partial X^{(k)}}\right) \mathfrak{X}_1^{(k)} \tag{53}$$

$$\Delta I_2^{(j)} = \left(\frac{\partial I^{(j)}}{\partial W}\right)_{\mathrm{Q}} \Delta W_2 + \left(\frac{\partial I^{(j)}}{\partial X^{(k)}}\right)_{\mathrm{Q}} \mathfrak{X}_2^{(k)} + \left(\frac{\partial^2 I^{(j)}}{\partial X^{(k)}\, \partial X^{(l)}}\right)_{\mathrm{Q}} \mathfrak{X}_1^{(k)} \mathfrak{X}_1^{(l)} + \left(\frac{\partial I^{(j)}}{\partial W}\right)_{\mathrm{Q}} \Delta W_1 \cdot \left(\frac{\partial I^{(j)}}{\partial X^{(k)}}\right)_{\mathrm{Q}} \mathfrak{X}_1^{(k)}, \tag{54}$$

and so on for larger n. We bring to the reader's attention the change in the symbol for derivatives, and its associated meaning. These derivatives are taken by treating the arguments of the function in Eq. (50) as *independent*, and a derivative with respect to one argument is taken by holding all other constant. As a result they do not remove G lines implicit in graphs for $X^{(2)}, X^{(3)}, \ldots$. In contrast, functional derivatives in Eq. (44) differentiate all arguments with respect to G and generate new diagrams including those that are topologically distinct from the ones differentiated. Thus the above $\Delta I_n^{(j)}$ do not couple to an infinite number of correlation functions; they couple only to the ones on which they explicitly depend. Furthermore, in this scheme $\Delta I_n^{(j)}$ are not related to each other by a chain of functional derivatives. In other words, while a functional derivative of $I^{(j)}$ with respect to G results in $I^{(j+1)}$, it does hold in general for the phenomenological $I^{(j)}$. In particular we have implicitly set $I^{(5)}=0$, and therefore manifestly break the hierarchy, i.e.,

$$I^{(j+1)} \neq \frac{\delta I^{(j)}}{\delta G}. \tag{55}$$

Substitution of these effective interactions in the BSE's forms a coupled set of integral equations, instead of functional-integrodifferential equations of the exact theory. Their solution yields a set of correlation functions $\{\mathfrak{X}_n^{(j)}\}$, which we now treat as fundamental; equations such as Eq. (23) then hold only approximately. Therefore in this approach the Kadanoff-Baym method for proving that the conservation laws that hold for G also hold for $X^{(2)}$, $X^{(3)}$, and so on is inapplicable.

Furthermore, in the exact theory, all correlation functions can be computed by functional differentiation of G, and this is equivalent to the statement that the self-energy can be expressed as a functional *only* of G. Clearly, the correlation functions calculated in the above scheme are no longer connected to G via functional derivatives, and this in turn im-

plies that the self-energy must be considered a functional of all the correlation functions upon which the effective interactions depend. Since one can still take quasiequilibrium self-energy to be a functional of G_{Q} alone, it acquires additional functional dependence on the deviations. In order to maintain the structure of the self-energy implied by the Dyson equation, we write

$$\Sigma = \Sigma[G_{\mathrm{Q}}, \mathfrak{X}_n^{(1)}, \mathfrak{X}_n^{(2)}], \tag{56}$$

so that it would produce the exact $\mathfrak{X}_n^{(1)}$ if the exact $\Delta I_n^{(j)}$ were used. As discussed in the next section, the equations of motion for $\mathfrak{X}_n^{(2)}$ and $\mathfrak{X}_n^{(3)}$ show that both these can be considered functionals of W_{Q}, $X_{\mathrm{Q}}^{(j)}$, and $\mathfrak{X}_m^{(1)}$. Therefore, if the correlation functions at quasiequilibrium can all be considered functionals of G_{Q}, then

$$\Sigma = \Sigma[G_{\mathrm{Q}}, \mathfrak{X}_n^{(1)}] = \Sigma[G]. \tag{57}$$

Thus Σ continues to be a functional of the nonequilibrium, but approximate G. This ensures that the nonequilibrium G calculated from this self-energy will give back the same self-energy. Thus the optical response, which only involves G explicitly, can be obtained self-consistently with the self-energy of the charges in the system.

It remains to determine which models for $\Delta I_n^{(j)}$ are admissible, and if one can follow a recipe to construct them. A formula for the simplest case, $\Delta I_1^{(2)}$, follows from the BSE and is discussed below in Sec. III C 2 [see Eq. (103)], but higher orders in the field are dictated by the particular system of charges to which the formalism is applied. However, we list some general rules to take into consideration. First, an important rule is the symmetry,

$$I^{(2)}(14;23) = I^{(2)}(41;32),$$

which is then inherited by the functions $\mathfrak{X}_n^{(2)}$. This symmetry implies that the two approximate equations of motion for $G(12)$ for coordinates 1 and 2 are exact conjugates of each other, and the particle number conservation follows when the equal time limit is taken.[14] We remark that this condition can be ensured by inspection of an approximate model for $I^{(2)}$ and symmetrizing it so that channels that are conjugates in the exact theory do remain conjugate in the approximate theory. Second, the approximate model must be able to capture the transient coherence and its subsequent loss. This coherence is nonlocal in the sense that it can be communicated across a time-lag via within the quasiparticle phase breaking time. In such a case, it is also necessary that the dynamic interaction, W, acts on all pairs of a correlation function symmetrically. That is, for a given correlation function $X^{(j)}$, each pair of one incoming and one outgoing line linked by W be equally weighted with the interaction among the outgoing and incoming lines. This is in contrast to solving the BSE in a *single* channel of ladder series by letting $I^{(2)}=W$ in Eq. (25). The explicit demonstration is deferred to II.

C. Equations of motion

In this section, we derive differential equations in the time variables of the deviations $\mathfrak{X}_n^{(j)}$ in the correlation functions $X^{(j)}$. The general strategy is to begin with an integral equation for $X^{(j)}$ [Figs. 2, 4(a), and 4(b)], apply a differential operator to it, and expand each function, O, in the resulting equation as $O_{\mathrm{Q}}+\Delta O$. The differential equation for $\mathfrak{X}_n^{(j)}$ then follows from the differential operator acting on $\Delta X^{(j)}$, and the remaining terms are classified as either couplings or sources.

To show the strategy, we first outline the derivation for single, and two particle correlation functions, $X^{(1)}=G$. We start with the general Dyson equation, writing $\Sigma=\Sigma_{\mathrm{Q}}+\Delta\Sigma$,

$$(G_0^{-1} - U_{\mathrm{Q}} - \Sigma_{\mathrm{Q}})G = 1 + (U + \Delta\Sigma)G,$$

and use the quasiequilibrium Dyson equation for G_{Q} to obtain

$$G_{\mathrm{Q}}^{-1}(11')G(1'2) = \delta(12) + [U(11') + \Delta\Sigma(11')]G(1'2).$$

Expanding G on both sides as $G_{\mathrm{Q}}+\Delta G$,

$$G_{\mathrm{Q}}^{-1}(11')\Delta G(1'2) = [U(11') + \Delta\Sigma(11')][G_{\mathrm{Q}}(1'2) + \Delta G(1'2)]. \tag{58}$$

The inverse function G_{Q}^{-1} is a differential operator written explicitly as

$$G_{\mathrm{Q}}^{-1}(11') = \left[i\frac{\partial}{\partial t_1} - H(1) \right]\delta(11') - U_{\mathrm{Q}}(11') - \Sigma_{\mathrm{Q}}(11'),$$

which yields Eq. (58) as a differential equation. The deviations ΔG and $\Delta\Sigma$ are expanded up to the desired order in the field, and by matching the terms of like orders we get the equation of motion for the correlation functions, $\mathfrak{X}_{1\ldots3}^{(1)}(12)$ in the first argument. Thus to the first order in U,

$$G_{\mathrm{Q}}^{-1}(11')\mathfrak{X}_1^{(1)}(1'2) - \Delta\Sigma_1(11')G_{\mathrm{Q}}(1'2) = U(11')G_{\mathrm{Q}}(1'2). \tag{59}$$

The self-energy deviation $\Delta\Sigma_1$ couples $\mathfrak{X}_1^{(1)}$ to $\mathfrak{X}_1^{(2)}$, and the equations for these two correlations have to be solved self-consistently. We will omit the equations for the latter until the next section. Once a solution is obtained for $\mathfrak{X}_1^{(j)}$ it can be substituted into the right hand side of the equation following from Eq. (58) that is second order in U,

$$G_{\mathrm{Q}}^{-1}(11')\mathfrak{X}_2^{(1)}(1'2) - \Delta\Sigma_2(11')G_{\mathrm{Q}}(1'2) = [U(11') + \Delta\Sigma_1(11')]\mathfrak{X}_1^{(1)}(1'2). \tag{60}$$

In both Eqs. (59) and (60), the left hand side consists of deviations of the same order in the field as the one being differentiated by application of G_{Q}^{-1}, while the right-hand side consists strictly of the deviations of lower orders. The left hand generates coupled linear dynamics of $\mathfrak{X}_n^{(j)}$, and the right hand side acts as a driving force, and we term the latter the source terms. Similarly, at the third order,

$$G_{\mathrm{Q}}^{-1}(11')\mathfrak{X}_3^{(1)}(1'2) - \Delta\Sigma_3(11')G_{\mathrm{Q}}(1'2) = [U(11') + \Delta\Sigma_1(11')]\mathfrak{X}_2^{(1)}(1'2) + \Delta\Sigma_2(11')\mathfrak{X}_1^{(1)}(1'2). \tag{61}$$

The nature of the couplings to $\mathfrak{X}_n^{(2\ldots3)}$ in these equations depends upon the approximation for the self-energy, which depends on the models picked for $I^{(j)}$. We will elaborate on

these couplings in the subsection below, and discuss the similar derivation for higher particle orders below.

The next equation in the hierarchy is the four-point BSE for $X^{(2)}=P$, and for which we write four equations in the form,

$$(G_{\mathrm{Q}}^{-1}-U-\Delta\Sigma)P=G+GI^{(2)}P,$$

where the operator on the left-hand side acts on one of the four arguments of P. This provides differential equations for evolution in each of the four time arguments of P. Again, expanding quantities on both sides as their quasiequilibrium value plus a deviation, and making use of the quasiequilibrium BSE, we obtain

$$(G_{\mathrm{Q}}^{-1}-U-\Delta\Sigma)\Delta P=\Delta G+\Delta GI^{(2)}P+G\Delta I^{(2)}P+GI^{(2)}\Delta P. \tag{62}$$

Expanding in the order of the field then yields equations for $\mathfrak{X}_n^{(2)}$, whose detailed form depends on $I^{(j)}$, and it is left to the subsections below. Similarly, the equations for $\Delta X^{(3\ldots4)}$ can be written using the BSE in 4b and applying G^{-1} to each external vertex. When the operator G^{-1} is acting on a quasiparticle diagram, it simply removes it. If it acts on a vertex of $X^{(2,\ldots3)}$, then the BSE for that correlation function is used to expand the term so that it contains a quasiparticle line at the vertex. This results in an equation for the time derivative of $X^{(j)}$, which is then expanded about the quasiequilibrium point as shown above to obtain an equation of motion for the deviations, $\mathfrak{X}_n^{(3)}$. While the above equations for ΔG and ΔP are derived without diagrams, the different contributions with proper counting are best determined using the diagrams where all permutations of the verticies and connections of the different components are explicit. This is the task to which we turn in the subsection below.

As we have seen in the case of $\mathfrak{X}_n^{(1)}$, the expansion yields equations of motion for $\mathfrak{X}_n^{(j)}$ consisting of terms that are linear combinations of $\mathfrak{X}_{n_n}^{(k)}$, which are the same order in the field, and products of $\mathfrak{X}_p^{(j)}\mathfrak{X}_{n-p}^{(j)}$, which are of the lower order in the field. Thus one starts by solving for $\mathfrak{X}_1^{(j)}$, which are driven by U only, and then uses these correlations to solve for $\mathfrak{X}_2^{(j)}$ and so on. Thus the equations for a given order form a *linear* system which are driven by the nonlinear interactions of correlation functions of lower order. The linearity arises from the perturbative treatment in the field amplitude. The driving terms would amalgamate with the homogeneous terms in a nonperturbative treatment leading to a full solution of the nonequilibrium many-body problem. Such a treatment is not attempted here.

Before presenting the results it is helpful to visualize the system of equations in abstract form. This also breaks down the derivation and presentation of the results into smaller components. The coefficients and source terms introduced below will be given in detail in the following two subsections. To first order in U,

$$i\frac{\partial}{\partial t_1}\mathfrak{X}_1^{(1)}(12)=\mathcal{M}_1^{(11;1)}\mathfrak{X}_1^{(1)}+\mathcal{M}_1^{(12;1)}\mathfrak{X}_1^{(2)}+\mathcal{S}_1^{(1;1)}, \tag{63}$$

$$i\frac{\partial}{\partial t_1}\mathfrak{X}_1^{(2)}(14;23)=\mathcal{M}_1^{(21;1)}\mathfrak{X}_1^{(1)}+\mathcal{M}_1^{(22;1)}\mathfrak{X}_1^{(2)}+\mathcal{M}_1^{(23;1)}\mathfrak{X}_1^{(3)}+\mathcal{S}_1^{(2;1)}, \tag{64}$$

$$i\frac{\partial}{\partial t_1}\mathfrak{X}_1^{(3)}(146;235)=\mathcal{M}_1^{(31;1)}\mathfrak{X}_1^{(1)}+\mathcal{M}_1^{(32;1)}\mathfrak{X}_1^{(2)}+\mathcal{M}_1^{(33;1)}\mathfrak{X}_1^{(3)}+\mathcal{S}_1^{(3;1)}, \tag{65}$$

where the $\mathcal{M}_n^{(jj';l)}$ describe coupling between the $\mathfrak{X}_1^{(n)}$, and the terms $\mathcal{S}_n^{(j;l)}$ are the sources. Here jj' in the superscript (left of semicolon) represent the particle order of the correlation functions, l stands for the time argument for which the differential equation is written, and n is the order in the external field. Here we have explicitly written the equations for just one time variable. For each $\mathfrak{X}^{(j)}$, there are $2j$ time variables and therefore $2j$ such first-order differential equations defined on the Keldysh contour. The couplings $\mathcal{M}$ for one of the times can be obtained from another by changing the appropriate arguments, and is done almost trivially from the self-energy diagrams. We will derive explicit forms for $\mathcal{M}$ for only t_1, and the relation to rest of the couplings will be made clear in the process. In the first equation, there is no explicit appearance of $\mathfrak{X}_1^{(3)}$, since the self-energy depends only on G and P. The third equation is where truncation is invoked to keep the system exact only up to the eight-point correlation functions. In the context of the previous section, we have explicitly neglected the dependence of all $I^{(j)}$ on $X^{(4)}$.

To second order we have

$$i\frac{\partial}{\partial t_1}\mathfrak{X}_2^{(1)}(12)=\mathcal{M}_2^{(11;1)}\mathfrak{X}_2^{(1)}+\mathcal{M}_2^{(12;1)}\mathfrak{X}_2^{(2)}+\mathcal{S}_2^{(1;1)}, \tag{66}$$

$$i\frac{\partial}{\partial t_1}\mathfrak{X}_2^{(2)}(14;23)=\mathcal{M}_2^{(21;1)}\mathfrak{X}_2^{(1)}+\mathcal{M}_2^{(22;1)}\mathfrak{X}_2^{(2)}+\mathcal{S}_2^{(2;1)}, \tag{67}$$

and to third order, there are only the single-particle Dyson equations,

$$i\frac{\partial}{\partial t_1}\mathfrak{X}_3^{(1)}(12)=\mathcal{M}_3^{(11;1)}\mathfrak{X}_3^{(1)}+\mathcal{S}_3^{(1;1)}, \tag{68}$$

whose solution determines the polarization signal that would be observed. The sum of the coupling terms in each of the above differential equations map the $\{\mathfrak{X}_n^{(j)}\}$ to itself. We thus refer to these terms collectively as *dynamical maps*. While leaving most of the details to Appendices, we provide an outline of the derivation of the maps and sources below, and focus on putting the results in the context of two-dimensional Fourier spectroscopy.

1. Dynamical maps

In this section, we identify the expressions for the couplings, $\mathcal{M}_n^{(ij;l)}$. In particular, we will use the diagrammatic BSE's to find the contributions to the $\Delta\Sigma_n$ terms in Eqs. (59)–(61) above, as well as the analogous terms in the equa-

tions for $\mathfrak{X}_n^{(2)}$. The expansion for $\Delta\Sigma$ follows immediately from Eqs. (C4)–(C6) of Appendix C, where the equation for the n^{th} order derivative of Σ is contracted with n factors of U to obtain $\Delta\Sigma_n$. In Figs. 2, 4(a), and 4(b) we have placed these terms on the left-hand side where all $X^{(j)}$ functions are connected to the right of effective interaction blobs. Each of these is contracted with a U on its free pair of vertices. Thus these diagrams in Figs. 2, 4(a), and 4(b) yield $\Delta\Sigma_1$, $\Delta\Sigma_2$, and $\Delta\Sigma_3$, respectively. While this prescription provides general expressions for $\Delta\Sigma_n$, we still need expressions for $\Delta I^{(j)}$ for BSE's for higher order correlation functions. One strategy is to leave the equations in the form of Eqs. (59)–(62) above, and then directly substitute the model effective interactions. However, the general expressions (26), (31), and (44) can be exploited further to identify contributions of different types of interactions. The extra effort provides insight into how $\Delta\Sigma$, and $\Delta I^{(j)}$ must couple different $\mathfrak{X}_n^{(j)}$ in any model for effective interactions. Models for effective interactions would inevitably include only a few scattering channels. In the following we also discuss the relative importance, in various quasiequilibrium states, of different scattering channels appearing explicitly in the general expressions.

To proceed we note that terms such as $\Delta I_n^{(j)}$ in higher order correlation functions can be obtained by expanding the corresponding BSE's in a form analogous to Eq. (43). The couplings originate from terms containing a single $\mathfrak{X}_n^{(j)}$ multiplied by a function that is evaluated in the quasiequilibrium state. In the diagrammatic form all n fields are placed on the *same* correlation box, $X^{(j)}$, which convert it into the deviation $\mathfrak{X}_n^{(j-n)}$.

For the single-particle correlation functions, we have

$$\mathcal{M}_n^{(11;1)}\mathfrak{X}_n^{(1)} = \mathcal{H}(11')\mathfrak{X}_n^{(1)}(1'2) + [\mathcal{W}^{(1)}(12|1'2') + \mathcal{K}^{(11;1)}(12|1'2')]\mathfrak{X}_n^{(1)}(1'2'), \tag{69}$$

$$\mathcal{M}_n^{(12;1)}\mathfrak{X}_n^{(2)} = [\mathcal{K}^{(12;1)}(12|1'4';2'3')]\mathfrak{X}_n^{(2)}(1'4';2'3'). \tag{70}$$

Here we have introduced several new quantities,

$$\mathcal{H}(11') = H(1)\delta(11') + \Sigma_{\mathrm{Q}}(11'), \tag{71}$$

$$\mathcal{W}^{(1)}(12|1'2') = i\int W_{\mathrm{Q}}(13;3'1')\Gamma_{\mathrm{Q}}(2'3';2''3)G_{\mathrm{Q}}(2''2), \tag{72}$$

$$\mathcal{K}^{(11;1)}(12|1'2') = i\int W_{\mathrm{Q}}(13;3'3'')G_{\mathrm{Q}}(3''1'')\times\left(\frac{\partial\Gamma(1''3';2''3)}{\partial X^{(1)}(1'2')}\right)_{\mathrm{Q}} G_{\mathrm{Q}}(2''2), \tag{73}$$

$$\mathcal{K}^{(12;1)}(12|1'4';2'3') = i\int W_{\mathrm{Q}}(15;5'3'')G_{\mathrm{Q}}(3''1'')\times\left(\frac{\partial\Gamma(1''5';2''5)}{\partial X^{(2)}(1'4';2'3')}\right)_{\mathrm{Q}} G_{\mathrm{Q}}(2''2) + \mathcal{K}_e^{(12;1)}(12|1'4';2'3'), \tag{74}$$

which depend only on the quasiequilibrium state. If Coulomb assisted band-to-band transitions are ignored, the kernel $\mathcal{K}_e^{(12;l)}$ exists only at even orders in the field, and corresponds to the variation of the dynamical susceptibility due to the optical excitation. The deviation in the dynamical potential has been given in Eqs. (51) and (52). A part of it contributes to the source terms, and the part that contributes to the dynamical map is

$$\Delta W_n(14;23)|_{map} = -iW_{\mathrm{Q}}(12';1'3)\mathfrak{X}_n^{(2)}(1'4';2'3')W_{\mathrm{Q}}(3'4;24') \tag{75}$$

and substituting this in the self-energy expression we obtain

$$\mathcal{K}_e^{(12;1)}(12|1'4';2'3') = \int W_{\mathrm{Q}}(12';1'7)W_{\mathrm{Q}}(3'5;64')G_{\mathrm{Q}}(77')\Gamma_{\mathrm{Q}}(7'6;25). \tag{76}$$

Similarly, the maps $\mathcal{M}_n^{(1j;2)}$ are obtained from the adjoint Dyson equation, and it produces

$$\mathcal{M}_n^{(11;2)}\mathfrak{X}_n^{(1)} = \mathfrak{X}_n^{(1)}(12)\mathcal{H}(2'2) + [\mathcal{W}^{(2)}(12|1'2') + \mathcal{K}^{(11;2)}(12|1'2')]\mathfrak{X}_n^{(1)}(1'2'), \tag{77}$$

$$\mathcal{M}_n^{(12;2)}\mathfrak{X}_n^{(2)} = [\mathcal{K}^{(12;2)}(12|1'4';2'3')]\mathfrak{X}_n^{(2)}(1'4';2'3'). \tag{78}$$

The different components are

$$\mathcal{W}^{(2)}(12|1'2') = i\int G_{\mathrm{Q}}(11'')\Gamma_{\mathrm{Q}}(1''3';1'3)W_{\mathrm{Q}}(2'3;3'2), \tag{79}$$

$$\mathcal{K}^{(11;2)}(12|1'2') = i\int G_{\mathrm{Q}}(11'')\times\left(\frac{\partial\Gamma(1''3';2''3)}{\partial X^{(1)}(1'2')}\right)_{\mathrm{Q}} G_{\mathrm{Q}}(2''3'')W_{\mathrm{Q}}(3''3;3'2), \tag{80}$$

$$\mathcal{K}^{(12;2)}(12|1'4';2'3') = i\int G(11'')\left(\frac{\partial\Gamma(1''5';2''5)}{\partial X^{(1)}(1'4';2'3')}\right)_{\mathrm{Q}}\times G_{\mathrm{Q}}(2''3'')W_{\mathrm{Q}}(3''5;5'2) + \mathcal{K}_e^{(12;1)}(12|1'4';2'3'). \tag{81}$$

For $\mathfrak{X}_n^{(2)}$, the integral form of the equation, without source terms, is derived in Eq. (E3) of Appendix E. Applying the

inverse Green function, G_{Q}^{-1}, to this equation at each of the four arguments generates the four evolution equations corresponding to the maps $\mathcal{M}_n^{(jj';l)}$. From Eq. (E3), we can now identify the components of the dynamical maps as follows:

$$\mathcal{M}_n^{(22;1)}\mathfrak{X}_n^{(2)} = \mathcal{H}(11')\mathfrak{X}_n^{(2)}(1'4;23) + G_{\mathrm{Q}}(2''2)I_{\mathrm{Q}}^{(2)}(12';2''1')\mathfrak{X}_n^{(2)}(1'4;2'3) + \mathcal{K}^{(22;1)}(14;23|1'4';2'3')\mathfrak{X}_n^{(2)}(1'4';2'3'), \tag{82}$$

$$\mathcal{M}_n^{(21;1)}\mathfrak{X}_n^{(1)} = [\delta(22')\delta(1'4) + \mathcal{K}^{(21;1)}(14;23|1'2')] \times \mathfrak{X}_n^{(1)}(1'2'), \tag{83}$$

$$\mathcal{M}_n^{(23;1)}\mathfrak{X}_n^{(3)} = \mathcal{K}^{(23;1)}(14;23|1'4'6';2'3'5') \times \mathfrak{X}_n^{(3)}(1'4'6';2'3'5'). \tag{84}$$

Due to termination of the hierarchy, the map $\mathcal{M}_n^{(23;1)}$ is set equal to zero for $n > N-2$ for $O(U^N)$ calculation.

The three kernels $\mathcal{K}^{(ij;1)}$ are given by the following expressions:

$$\mathcal{K}^{(22;1)}(14;23|1'4';2'3') = G_{\mathrm{Q}}^{-1}(11'')\left(\frac{\partial I^{(2)r}(1''4'';23'')}{\partial X^{(2)}(1'4';2'3')}\right)_{\mathrm{Q}}\Gamma_{\mathrm{Q}}(3''4;4''3) + \mathcal{K}_{22}^{e}(14;23|1'4';2'3') \tag{85}$$

$$\mathcal{K}^{(23;1)}(14;23|1'4'6';2'3'5') = G_{\mathrm{Q}}^{-1}(11'')\left(\frac{\partial I^{(2)r}(1''4'';23'')}{\partial X^{(3)}(1'4'6';2'3'5')}\right)_{\mathrm{Q}}\Gamma_{\mathrm{Q}}(3''4;4''3), \tag{86}$$

$$\begin{aligned}\mathcal{K}^{(21;1)}(14;23|1'2') &= G_{\mathrm{Q}}^{-1}(11')G_{\mathrm{Q}}(2''2)\Gamma_{\mathrm{Q}}(2'4;2''3) \\ &- G_{\mathrm{Q}}^{-1}(11'')(P_{\mathrm{Q}}^{0}I_{\mathrm{Q}}^{(2)})(1''4';21')G_{\mathrm{Q}}(4'4'')\Gamma_{\mathrm{Q}}(2'4;4'3) \\ &- G_{\mathrm{Q}}^{-1}(11'')(P_{\mathrm{Q}}^{0}I_{\mathrm{Q}}^{(2)})(1''2';23'')G_{\mathrm{Q}}(3''3')\Gamma_{\mathrm{Q}}(3'4;1'3) \\ &+ G_{\mathrm{Q}}^{-1}(11'')\left(\frac{\partial I^{(2)r}(1''4'';23'')}{\partial X^{(1)}(1'2')}\right)_{\mathrm{Q}}.\end{aligned} \tag{87}$$

The function $I^{(2)r}$ is the reducible interaction,

$$I^{(2)r}(14;23) = P^{(0)}(12';21')T^{(2)}(1'4';2'3')P^{(0)}(3'4;4'3), \tag{88}$$

and where $P^{(0)}$ has been defined earlier in Eq. (28). The partial derivative of $I^{(2)r}$ with respect to $X^{(2)}$ appears in Eq. (85), which is ultimately substituted in Eq. (82). There, in the last term, it multiplies $\mathfrak{X}_n^{(2)}$, and a yields contribution of the latter to $\Delta I_n^{(2)r}$ via Eq. (54). This contribution of $\mathfrak{X}_n^{(2)}$ to $\Delta I_n^{(2)r}$ is shown diagrammatically in Figs. 6(a) and 6(c). The middle terms in Eq. (87) for $\mathcal{K}^{(21;1)}$ are necessary to cancel the overcounting done by the use of $I^{(2)r}$, and they are obtained by replacing the quasiparticle arrows attached to one of the four

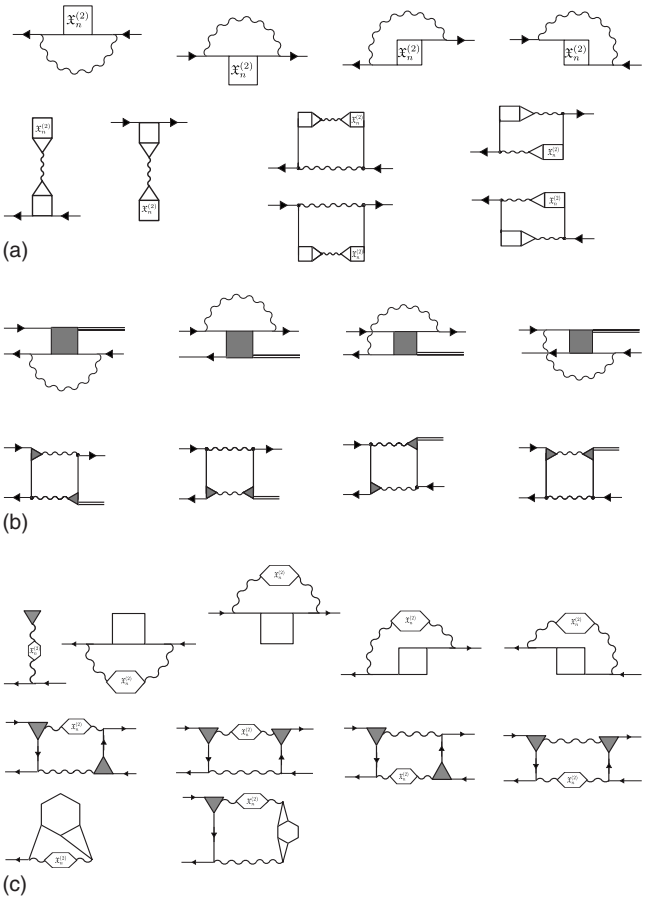

FIG. 6. Contributions of two-particle correlations to the two-particle EOM.

vertices by $\mathfrak{X}_n^{(1)}$. Their diagrammatic form is shown in Fig. 6(b). The kernel $\mathcal{K}^{(23;1)}$ is obtained by setting the two terms with six-point correlation functions in $I^{(2)}$ to $\mathfrak{X}_n^{(3)}$. In contrast to diagrams in Fig. 3, Fig. 6(a) explicitly shows $I^{(2)}$ symmetrically, and the substitution of the resulting two-particle correlation back into the self-energy would ensure that particle number conservation holds.

The map $\mathcal{M}_n^{(jj';2)}$ is obtained by acting on the argument 2 in Eq. (E3) by G_{Q}^{-1}. We obtain

$$\mathcal{M}_n^{(22;2)}\mathfrak{X}_n^{(2)} = \mathfrak{X}_n^{(2)}(14;2'3)\mathcal{H}(2'2) + G_{\mathrm{Q}}(11'')I_{\mathrm{Q}}^{(2)}(1''2';21')\mathfrak{X}_n^{(2)}(1'4;2'3) + \mathcal{K}^{(22;2)}(14;23|1'4';2'3')\mathfrak{X}_n^{(2)}(1'4';2'3'), \tag{89}$$

$$\mathcal{M}_n^{(21;2)}\mathfrak{X}_n^{(1)} = [\delta(11')\delta(2'3) + \mathcal{K}^{(21;1)}(14;23|1'2')] \times \mathfrak{X}_n^{(1)}(1'2'), \tag{90}$$

$$\mathcal{M}_n^{(23;2)}\mathfrak{X}_n^{(3)} = \mathcal{K}^{(23;1)}(14;23|1'4'6';2'3'5') \times \mathfrak{X}_n^{(3)}(1'4'6';2'3'5'). \tag{91}$$

Here the kernels $\mathcal{K}^{(ij;2)}$ are given by

$$\mathcal{K}^{(22;2)}(14;23|1'4';2'3') = \left(\frac{\partial I^{(2)r}(14'';2''3'')}{\partial X^{(2)}(1'4';2'3')}\right)_{\mathrm{Q}} G_{\mathrm{Q}}^{-1}(2''2)\Gamma_{\mathrm{Q}}(3''4;4''3) + \mathcal{K}_{22}^{e}(14;23|1'4';2'3') \tag{92}$$

$$\mathcal{K}^{(23;2)}(14;23|1'4'6';2'3'5') = \left(\frac{\partial I^{(2)r}(14'';2''3'')}{\partial X^{(3)}(1'4'6';2'3'5')}\right)_{\mathrm{Q}} G_{\mathrm{Q}}^{-1}(2''2)\Gamma_{\mathrm{Q}}(3''4;4''3), \tag{93}$$

$$\begin{aligned}\mathcal{K}^{(21;2)}(14;23|1'2') &= G_{\mathrm{Q}}^{-1}(2'2)G_{\mathrm{Q}}(11'')\Gamma_{\mathrm{Q}}(1''4;1'3) \\ &- (P_{\mathrm{Q}}^{0}I_{\mathrm{Q}}^{(2)})(14'';2''1')G_{\mathrm{Q}}^{-1}(2''2)G_{\mathrm{Q}}(4'4'')\Gamma_{\mathrm{Q}}(2'4;4'3) \\ &- (P_{\mathrm{Q}}^{0}I_{\mathrm{Q}}^{(2)})(12';2''3'')G_{\mathrm{Q}}^{-1}(2''2)G_{\mathrm{Q}}(3''3')\Gamma_{\mathrm{Q}}(3'4;1'3) \\ &+ \left(\frac{\partial I^{(2)r}(1''4'';23'')}{\partial X^{(1)}(1'2')}\right)_{\mathrm{Q}} G_{\mathrm{Q}}^{-1}(2''2).\end{aligned} \tag{94}$$

The maps, or equations for the variables 3 and 4, are obtained by exploiting the symmetry condition, $X^{(2)}(14;23)=X^{(2)}(41;32)$. Diagrammatically, this amounts to flipping the diagrams left to right and then upside down.

The diagrams shown in Figs. 6(a) contribute to Eqs. (82) and (89), while those in Fig. 6(b) contribute to Eqs. (83) and (90). We now briefly discuss their connection to decoherence. These diagrams originate from those for $I^{(2)}$ shown in Fig. 3, and discussed briefly at the end of Sec. II C. The kernel $\mathcal{K}^{(22;l)}$, and the subtracted terms in $\mathcal{K}^{(21;l)}$ are shown diagrammatically in Figs. 6(a) and 6(b), respectively, but without the application of G_{Q}^{-1}. Figure 6(a) shows three classes of diagrams. The top line shows retarded interaction in the *particle-hole channel* in such a way that a full correlation develops between the times this retarded interaction travels. The term particle-hole channel is meant to describe a pair of particles antiparallel in time. Thus these diagrams in a sense measure the state of the correlation both at a creation and annihilation, or, heuristically, the "bra" and "ket" state of the two-particle density matrix. The retarded interaction in fact contains a susceptibility bubble that represents the interaction of this composite particle with an external electron, and traced over this external particle. Taking into account the propagators in the polarization bubble, we can also view this term as a three-particle Green function traced over two of its arguments to form a four-point correlation function. In the context of transport problems, similar diagrams involving three-particle functions are also found for treating many-body correlations for plasmas, and in calculations of dielectric functions.[17,18] There the necessity for the three-particle function arises from a density high enough that three-particle scattering is important. Here they are important even for a low density system in order to capture the subtle decoherence effects consistently. Appropriate excitation could put the system in a superposition of two states, and this superposition would undergo decoherence due to interactions. Because these interactions are dynamic, coherence can exist across a time delay and therefore between the incoming and outgoing particles of a temporally extended correlation function. Including all these diagrams on the same footing as the ladder series has dramatic effects on the calculation of the decoherence of excitons, as discussed in Sec. II. We also remark that decoherence in the picture developed so far arises from partially tracing over correlation functions in the higher particle Hilbert spaces. The bubble thus represents a kind of effective bath, and interacting with it the two-particle correlation can undergo decoherence.

The first two diagrams in the second line of Fig. 6(a) show the interaction in a particle-hole channel, which starts at W. This interaction is renormalized to produce the dynamic Coulomb interaction, and vertex corrections are inserted on both ends to account for self-interaction of the two different interacting particles. The two diagrams thus show the field-induced effects on these vertices. From the self-energy expressions, it follows that the $\mathfrak{X}_n^{(2)}(14;23)$ joins with the interaction line at 3,4, and therefore must satisfy $\zeta_3=\zeta_4$. The direct contribution of this term to the evolution of excitons thus occurs as field-induced changes in the particle-particle vertex. Their direct role in decoherence will appear at higher orders in Coulomb interaction. Finally, the rest of the four diagrams arise from the field-induced changes in the dynamical susceptibility. If Coulomb assisted transitions across the gap can be neglected, then these diagrams do not contribute directly in the horizontal particle-hole channel in the dynamical map. They will contribute if a coherence is present to flip the band type of electron as it travels from the bottom to top of the diagram. Thus these diagrams will only appear in the source terms when the calculation is restricted to the horizontal channel.

2. Source terms

Here we give the source terms at all three orders in the field in the integral form. They consist of the effective field U, and corrections arising from the optically induced correlation functions beyond the Hartree one. The sources $\mathcal{S}_n^{(j;l)}$ have already been identified in the equations of motion corresponding to time derivative in the argument l. For brevity, we will instead give explicit expressions for functions $\mathcal{S}_n^{(j)}$, which when acted on by G_{Q}^{-1} on the argument l yield $\mathcal{S}_n^{(j;l)}$,

$$\mathcal{S}_n^{(j;l)}(1\ldots l\ldots j;1'\ldots l'\ldots j') = G_{\mathrm{Q}}^{-1}(ll'')\mathcal{S}_n^{(j)}(1\ldots l''\ldots j;1'\ldots l'\ldots j'), \tag{95}$$

$$\mathcal{S}_n^{(j;l')}(1\ldots l\ldots j;1'\ldots l'\ldots j') = \mathcal{S}_n^{(j)}(1\ldots l\ldots j;1'\ldots l''\ldots j')G_{\mathrm{Q}}^{-1}(l''l'). \tag{96}$$

The explicit presence of $G_{\mathrm{Q}}(ll'')$ and $G_{\mathrm{Q}}(l''l)$ in the expressions below makes this operation trivial. Furthermore, this explicit presence also means that the source terms below form the leading term in a series solution to the dynamical Eqs. (63)–(68).

We have for the first order,

$$\mathcal{S}_1^{(1)}(12) = G_Q(11')U(11')G_Q(1'2), \tag{97}$$

which just describes propagation of free electron and a valence-band hole generated by the external field. At the second order, there start to appear local field corrections beyond the Hartree level. We denote this modification to U by

$$\mathcal{U}_n^{(1)}(12) = U(12)\delta_{n1} + \Delta\Sigma_n(12), \tag{98}$$

where $\Delta\Sigma_n$ is the deviation in self-energy that describes all possible interactions among the pairs generated by n pulses, and includes contributions from $\mathfrak{X}_m^{(j)}$ for $m<n$ only (see discussion at the beginning of Sec. III C 1). In general,

$$\Delta\Sigma_n(12) = W_Q(13;3'1')[\mathfrak{X}_n^{(1)}(1'1'')\Gamma_Q(1''3';23) + G_Q(1'1'')\Delta\Gamma_n(1''3';23)],$$

for odd n, and where $\Delta\Gamma_n$ is the corresponding deviation in the vertex function. For even n, we also have to include

$$\Delta W_{2n}(14;23) = -iW_Q(15;63)\mathfrak{X}_{2n}^{(2)}(66';55')W_Q(5'4;26') - iW_Q(15;63)\sum_{j=1}^{n-1}\mathfrak{X}_{2n}^{(2)}(66';55')\Delta W_{2(n-j)} \times(5'4;26'),$$

where we have used Eq. (51). Thus we write the second-order source as

$$\mathcal{S}_2^{(1)}(12) = G_Q(11')\mathcal{U}_1^{(1)}(1'1'')G_Q(1''2')\mathcal{U}_1^{(1)}(2'2'')G_Q(2''2). \tag{99}$$

Similarly, the third order source $\mathcal{S}_3^{(1)}$ has the analogous form,

$$\mathcal{S}_3^{(1)}(12) = G_Q(11')\mathcal{U}_2^{(1)}(1'1'')G_Q(1''2')\mathcal{U}_1^{(1)}(2'2'')G_Q(2''2) + G_Q(11')\mathcal{U}_1^{(1)}(1'1'')G_Q(1''2')\mathcal{U}_2^{(1)}(2'2'')G_Q(2''2) + G_Q(11')\mathcal{U}_1^{(1)}(1'1'')G_Q(1''3')\mathcal{U}_1^{(1)} \times(3'3'')G_Q(3''2')\mathcal{U}_1^{(1)}(2'2'')G_Q(2''2). \tag{100}$$

Next we consider $\mathcal{S}_n^{(2)}$, which gives rise to the formation of excitons and the coherence among their states. To the first order

$$\mathcal{S}_1^{(2)}(14;23) = \{\mathcal{S}_1^{(1)}(11')G_Q(2'2) + \mathcal{S}_1^{(1)} \times(2'2)G_Q(11')\}\Gamma_Q(1'4;2'3). \tag{101}$$

To obtain $\mathcal{S}_2^{(2)}$, we contract the eight-point diagrams in Fig. 4 with two field lines, not connecting two separate correlation functions with a field line; this rule is explained in the next section. Proceeding in this manner we get the expression,

$$\mathcal{S}_2^{(2)}(14;23) = G_Q(11')\mathcal{U}_1^{(1)}(1'3')G_Q(3'1'')G_Q(2''4')\mathcal{U}_1^{(1)} \times(4'2')G_Q(2'2)\Gamma_Q(1''4;2''3) + G_Q(11')\mathcal{U}_1^{(1)} \times(1'1'')I_Q^{(2)}(1''4';2'3')\mathfrak{X}_1^{(2)}(3'4;4'3)G_Q(2'2) + G_Q(11')I_Q^{(2)}(1'4';2'3')\mathfrak{X}_1^{(2)}(3'4'';4'3)\mathcal{U}_1^{(1)} \times(4''2'')G_Q(2''2) + G_Q(11')\mathcal{U}_1^{(1)}(1'1'')\Delta I_1^{(2)} \times(1''4';2'3')X_Q^{(2)}(3'4;4'3)G_Q(2'2) + G_Q(11')\Delta I_1^{(2)}(1'4';2''3')\mathcal{U}_1^{(1)}(2''2')X_Q^{(2)} \times(\times 3'4;4'3)G_Q(2'2). \tag{102}$$

Here $\Delta I_1^{(2)}$ is the $O(U)$ variation induced in the effective interaction, and it can be related explicitly to the inverse functionals of quasiequilibrium BSE, assuming they exist,

$$\Delta I_1^{(2)}(14;23) = P_Q^{-1}(12';21')\mathfrak{X}_1^{(2)}(1'4';2'3')P_Q^{-1}(3'4;4'3) - (P_Q^0)^{-1}(12';21')P_1^0(1'4';2'3') \times(P_Q^0)^{-1}(3'4;4'3). \tag{103}$$

Note that the term $\Delta I_1^{(2)}\mathfrak{X}_1^{(2)}$ is not present in Eq. (102) because it implicitly contains a partial summation that forces it to be a second-order deviation in Γ, and it has been included in the dynamical map above. It is now clear that the sources can be expressed algebraically in a compact form, and can be understood as successive corrections to the Hartree renormalization of the driving field.

We now come back to the point raised earlier [Eq. (57)] that Σ may be considered a functional of G only. Since all couplings are linear, they remain functionals of G_Q so long as the quasiequilibrium problem is formulated to ensure that $\Sigma_Q=\Sigma_Q[G_Q]$. Therefore, when the coupled equations are solved, the solutions are functionals of G_Q and whatever functions the sources depend on. Consider now the solution of the first-order equations driven by the sources in Eq. (97), and Eq. (99) above as well as $\mathcal{S}_1^{(3)}$ not shown here explicitly. The latter is a function of G_Q, $\mathcal{S}_1^{(1)}$, and $\mathcal{S}_2^{(1)}$, and by Eq. (99) it may be considered a function of G_Q and U alone. Therefore all $\mathfrak{X}_1^{(j)}$ can be considered functionals of G_Q and U. When the sources for the second-order equations are constructed, they are always expressible in terms of $\mathfrak{X}_1^{(j)}$, and similarly the third order sources in terms of $\mathfrak{X}_1^{(j)}$ and $\mathfrak{X}_2^{(j)}$. Consequently, all $\mathfrak{X}_n^{(j)}$ can be considered functionals of G_Q and U. Assuming that the dependence of ΔG on U is invertible, they may in turn be considered functionals of the nonequilibrium G alone.

IV. EXPERIMENTAL SCENARIOS

A. External and effective fields

The bare source that drives interband coherence is taken within the dipole approximation, and thus is of the form,

$$\Phi_{cv}(12) = \phi_{cv}(\boldsymbol{k}_1,t_1)\delta(t_1-t_2)\delta(\boldsymbol{k}_1-\boldsymbol{k}_2)\delta_{\sigma_1\sigma_2}, \tag{104}$$

For convenience we have written the band indices corresponding the arguments of Φ as subscripts. The subscript c corresponds to the conduction band, and v to the valence band. Here $\phi_{cv}(\boldsymbol{k},t_1)=-e\hbar^{-1}\boldsymbol{\xi}(\boldsymbol{k})\cdot\mathcal{E}(t)e^{-i\omega t}$ is the effective amplitude for making the interband transition, and the wave vector is the same for initial and final state due to negligible momentum of the optical field: $\boldsymbol{k}_1=\boldsymbol{k}_2=\boldsymbol{k}$. The positive frequency component of the electric field $\mathcal{E}(t)e^{-i\omega t}$ is the macroscopic field inside the medium of quantum well with a dielectric constant different from unity, and with a center frequency ω. The discussion below refers to fields inside the well (see Appendix A to obtain fields outside the well).

This particular identification of bands is useful only for normal insulators and semiconductors, where there is an energy gap between the ground state and the lowest excited state. In the presence of Coulomb interactions, this imposes restrictions on the solutions of the Dyson equation and thus the single-particle self-energy. Within the framework of Green functions, the Dyson equation for the system in thermodynamic equilibrium takes the form,

$$[E - H_0(\boldsymbol{r})]G(\boldsymbol{r},\boldsymbol{r}';E) - \int d\boldsymbol{r}''\Sigma(\boldsymbol{r},\boldsymbol{r}'';E)G(\boldsymbol{r}'',\boldsymbol{r};E) = \delta(\boldsymbol{r}-\boldsymbol{r}'). \tag{105}$$

In general, the solution to this equation consists of isolated, and perhaps also a continuous, set of poles in the complex plane. If no poles exist in a finite interval on the real axis (or close to it), then that interval may be identified with an energy gap. The solutions with isolated poles close to the real axis, and to the right of this gap then define a set of conduction states in which a quasiparticle can freely propagate over a time interval corresponding to the imaginary part of the pole. Similarly isolated poles to the left of the gap in the complex plane define valence states that are all filled by quasiparticles in the ground state. The formal manipulations of the preceding sections are independent of these considerations, but the restrictions like these are necessary steps in actual calculations. Without any interaction induced symmetry breaking, the quasiparticle wave functions will also obey the lattice symmetry, and a crystal momentum can be associated with them. In this sense the description of the semiconductor via energy bands survives. Clearly these single-particle concepts remain useful only at time scales shorter than the lifetime set by the imaginary self-energy.

Assuming the many-body system to be a semiconductor, the effective field, U, is given by

$$U_{\zeta_1\zeta_2}(\boldsymbol{k},t_1;\boldsymbol{k},t_2) = \Phi_{cv}(\boldsymbol{k},t_1;\boldsymbol{k},t_2)\delta_{\zeta_1 c}\delta_{\zeta_2 v} - \int V_{\zeta_1\zeta_3;\zeta_4\zeta_2}(13;42) \times \frac{\delta G(43)}{\delta\Phi_{cv}(3'4')}\phi_{cv\boldsymbol{k}}(t_3')\delta(t_3'-t_4'),$$

where we have not fixed the band subscripts on U, since in general, the second term on right-hand side may couple the interband transitions to each other and to the intraband motion. This term represents the contribution made by the change in the Hartree energy of the electron gas due to the creation of electron-hole pairs. We first consider the modification of the interband transitions between the conduction and the valence bands,

$$U_{cv}(\boldsymbol{k},t_1;\boldsymbol{k},t_2) - \Phi_{cv}(\boldsymbol{k},t_1;\boldsymbol{k},t_2) = -\int V_{c\zeta_3;\zeta_4 v}(13;42)\frac{\delta G(43)}{\delta\Phi_{cv}(3'4')}\phi_{cv\boldsymbol{k}}(t_3')\delta(t_3'-t_4').$$

By Eqs. (6)–(8), only the Umklapp processes contribute to the matrix element $V_{c\zeta_3;\zeta_4 v}(13;42)$ close to $\boldsymbol{k}=0$ (Γ point). This is so because in this region the cell-periodic functions $u_\zeta(\boldsymbol{k};\boldsymbol{\rho},z)$ can be taken approximately equal to $u_\zeta(\boldsymbol{0};\boldsymbol{\rho},z)$, where the latter belonging to different bands are orthogonal. If all relevant dynamics is concentrated in a small enough region around the Γ point, then the matrix elements of interest involve only $u_\zeta(\boldsymbol{0};\boldsymbol{\rho},z)$ to a good approximation. In essence the particular Umklapp processes that allow Coulomb interaction to drive interband transitions can resonate with optical excitation close to the band edge in general. However, neglecting that is a good approximation for most problems of interest, such as exciton dynamics. This also holds for the intraband terms, U_{cc} and U_{vv} because in the response function $\delta G/\delta U$, they require either an Umklapp process at the 34 coordinate of V, or a band transition other than the one driven by the field by the field. Since we only consider Coulomb interaction, the Umklapp process is also the only choice for the latter that is consistent with the Hamiltonian. Therefore, we assume that the dielectric function arising from Eq. (19), which connects the bare field with the Maxwell field, is unity at band-gap frequencies and diagonal in band indices. More generally, transitions among subbands, which can be low in energy, can couple to the low energy excitations of the charge density and the functions U_{cv} and Φ_{cv} will become substantially different.

B. Analysis via diagrams

In the foregoing we have obtained differential equations for $\mathfrak{X}_n^{(j)}$ that consist of dynamical maps and source terms driving them. Formally, a series solution to these equations begins with an integral of the source terms, which corresponds to $\mathcal{S}_n^{(j)}$ in Sec. III C. This approximate solution neglects the couplings. The effect of the couplings can be treated by iteration. The iteration generates a series of terms that represent propagation at the external vertices, and interactions among those vertices in all possible ways. A contribution to the solution can be represented diagrammatically to depict the physical processes it entails. Without interactions, a finite number of diagrams, namely, the double-sided Feynman diagrams, capture the full solution. With interactions, the set of such diagrams is infinite, and it is not practical to represent the entire solution diagrammatically.

It is practical, however, to use a diagrammatic form to represent the simplest term in the series, the $\mathcal{S}_n^{(j)}$. Diagrams provide an intuitive yet rigorous method for understanding the sources that drive the dynamics of a particular $\mathfrak{X}_n^{(j)}$. They also provide an extremely useful pedagogical tool to build approximate solutions, and identify their qualitative aspects. Furthermore, since the sources are those components in the equations that relate directly to the experimental parameters for pulses, they allow one to depict an experimental scenario as well. In particular, different subsets of diagrams are distinguished as dominant under different excitation conditions corresponding to pulse sequences and choice of observation directions. Recalling the relation in Eq. (14), the branch indices and particle species lying on the two contours at observation time t are also fixed by the experiment. So a connection with experiment can be made directly using the diagrams. In the rest of this section we develop a set of rules to construct diagrams, which can be applied to either sources or solutions. Note that we have already encountered a set of diagrams in the previous sections. Those diagrams are gen-

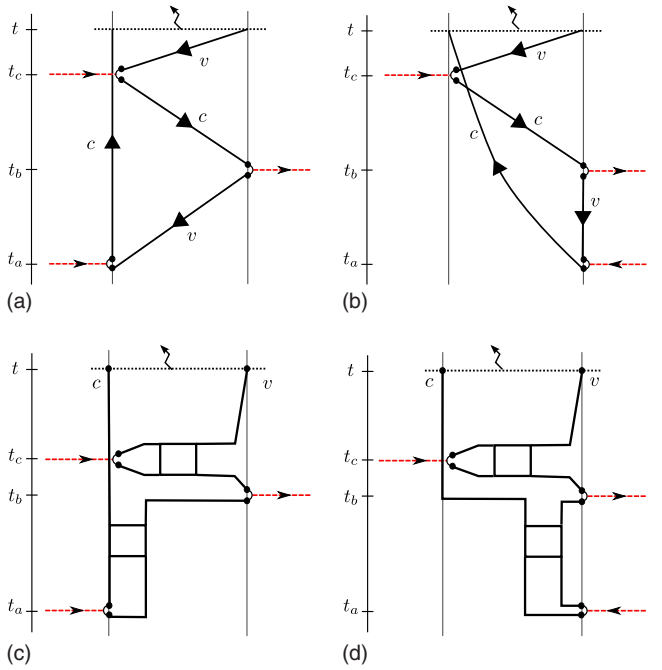

FIG. 7. (Color online) Pair evolution induced by three pulses, where the pairs are either uncorrelated (top) or correlated (bottom).

eral, but not explicit in the contour branch indices, pulse sequences, and absorption/emission of the electromagnetic fields.

In developing the diagrams, we assume that the rotating wave approximation holds so that we are close to a resonance in the system and the optical cycle is much shorter than the time scales in which we are interested. The diagrams are represented on Keldysh contours oriented vertically with time increasing upwards. The left contour is positive, and the right is negative, as shown in Fig. 7. We represent the self-consistent potential, U, by a directed dashed line, where the line entering the diagram represents the unconjugated field that is absorbed, and the line leaving the diagram is the conjugated field that is emitted by the system. The temporal location of these lines clearly exhibits the pulse sequence and time delays. The observed field emitted by the polarization is shown as a small arrow pointing out of the horizontal line placed at the observation time. The quasiparticle lines can either lie on the contours, parallel, or antiparallel to its direction, or can run from one contour to the other. In either case, if the arrow points against the contour direction, the field operators in the expectation value are reversed. They thus carry factors of density.

We now discuss rules for constructing these diagrams for the source terms $\mathcal{S}_n^{(j)}$ in the form in which G_Q lines terminate at all external vertices. The $\mathcal{S}_n^{(j;l)}$ may be obtained by removing the appropriate G_Q. Using the integral equations derived above and the expression Eq. (14) for the density matrix, it can be verified that admissible diagrams can be drawn via the following recipe.

(1) Draw the positive and negative contours, and place n electric-field vertices at desired points on the contour, with the arrow pointing outwards for fields that are conjugated, and inwards for the unconjugated fields.

(2) On the contour, mark the points $1,2,\ldots,j$ corresponding to the arguments of $\mathcal{S}_n^{(j)}$ function being represented. Fill the diagram via the following rules.

(3) Insert a diagram between the contours using either Fig. 1 to convert the mathematical expression into a diagram, or directly from the BSE for $X^{(j+n)}$ (Figs. 2 and 4). Attach the n external field lines to the diagrams, with a pair of vertices (other than those in rule 2) for each line. At the electric-field vertex, a conduction electron should leave and valence electron enter the vertex if the field line is incoming, and the opposite if the line is outgoing.

(4) The pair to which an external field line connects must belong to the same correlation under partial contraction. If a pulse fully contracts a diagram, i.e., it produces $\mathfrak{X}_{n;cv}^{(1)}$, then it is allowed to connect two otherwise separate parts of a diagram. The proof of this rule is in Appendix F.

(5) A correlation function can be connected to rest of the diagram only via effective interaction or a field line, and up to only two vertices may be attached to an interaction. This rule follows by examining Eqs. (C2) and (C3) and noting the placement of arguments in $\delta G/\delta U$ relative to $\delta\Sigma/\delta G$.

(6) A completed diagram with all three electric-field lines attached must not be in a separated form. This is because the final diagram represents a term in the expansion of single-particle Green function. The internal vertices are not placed on the contours but in the space between them.

(7) A diagram containing all three pulses must have a conduction electron (band index c) arriving at a point on the positive contour and a valence electron (band index v) departing from a point on the negative contour. The two points should be at equal real time. Note that this rule is a specialization of the formalism to semiconductors excited close to the gap frequencies.

(8) At this point, a diagram contains exactly one effective interaction blob since all BSE's are linear in the effective interaction. More interactions are placed only when iterating to build an approximate solution.

This produces a set of diagrams that contain products of correlation functions, effective interactions, and the self-consistent field. These diagrams are evaluated, and source diagrams are distinguished, by the following rules:

(a) For each $X^{(j)}$ connected directly to k instances of U, write $\mathfrak{X}_k^{(j-k)}$.

(b) For four-, six-, and eight-point blobs, write $I^{(2)}(11';21')$, $I^{(3)}(11'2';21''2'')$, and $I^{(4)}(11'2'3';21''2''3'')$, respectively, as given by Fig. 1.

(c) For each vertex where the field line is entering the diagram, assign $U_{cv}(\boldsymbol{k},t)$, and for each line leaving $U_{vc}(\boldsymbol{k},t)$ regardless of which contour the vertex lies on. Conserve the total quasimomentum at the field vertices as a consequence of the dipole approximation. Again, this rule is also a specialization to semiconductors excited close to the gap frequencies.

(d) Any vertex that is not on the final observation time, and not connected to the external fields is an internal vertex and must be summed over time, branch indices, particle species, and momenta.

(e) Some internal summations involving $I^{(j)}$ will be of the form where both arguments of $\mathfrak{X}_n^{(1)}$ are connected to the *same* $I^{(j)}$. To each diagram containing m functions,

$\mathfrak{X}^{(1)}_{n_1}, \mathfrak{X}^{(1)}_{n_2}, \ldots \mathfrak{X}^{(1)}_{n_m}$, connected to $I^{(j)}$ in this form, associate $n \equiv \sum_{i=1}^{m} n_i$, and $p \equiv j-m$. Collect all diagrams that have the same n and p, and substitute for all of them a single diagram with $I^{(j)}$ replaced by $\Delta I^{(p)}_n$. It is always possible to do this if all possible diagrams are constructed with proper counting such that the diagrams are identical if the $I^{(j)}$ and $\mathfrak{X}^{(1)}_{n_i}$ identified above are removed. The reason for this is simple: these diagrams result from derivatives of $I^{(p)}$.

(f) Set the remaining correlations to their quasiequilibrium values.

(g) If a diagram corresponds to a source term, $\mathcal{S}^{(j)}_n$, then it must not have any component that is $O(U^n)$, and its external vertices must all be connected to $X^{(n)}_{\mathrm{Q}}$ or G_{Q}. The latter can be ensured by iterating BSE of a correlation function as described below Eq. (62). Remove the G_{Q} line from the contribution to EOM for the corresponding vertex.

(h) Among the remaining $X^{(n)}_{\mathrm{Q}}$, there will be up to j connected directly to j pulses. Express these as $\mathfrak{X}^{(n-1)}_1$.

(i) Using the model for $I^{(j)}$, substitute the model expressions for $\Delta I^{(j)}_n$ as given by Eqs. (52)–(54).

In a chemical picture, where the focus is on excitons, biexcitons, and the like, certain correlation functions are identified with particles of new species. It is often desirable, and quite simple, to determine whether a diagram is proportional to the density of a particular species using the following auxiliary rules:

(a) Any quasiparticle line directed *against* the contour is proportional to the density of that quasiparticle species.

(b) For any correlation function, if traveling along the contour one encounters a creation point before the annihilation point, then either (a) the diagram is proportional to the density of quasiparticle related to the two points, or (b) if all constituents of a composite particle species are annihilated before they are created, the diagram is proportional to the density of species in question.

We illustrate the *conversion* of a diagram to a mathematical expression by discussing some example diagrams. The *construction* of source diagrams will be illustrated using a concrete example in Sec. IV C below.

The diagrams we discuss now are some arbitrarily chosen contributions to $\mathfrak{X}^{(1)}_{3;cv}(12)$ for the case of three pulses a,b,c, and the observation direction corresponding to $\omega_a-\omega_b+\omega_c$. Depending on the contour on which the fields are placed, there are eight combinations. In the DCT formalism, only the diagrams where the first pulse is placed on the left contribute, due to the electron-hole vacuum as the ground state; this is essentially the content of the Axt-Stahl theorem.[8] In the diagrams where the first pulse is on the right the quasiparticle propagators at the first pulse will always be anticontour ordered, and would thus be given by the removal amplitudes. Consequently these diagrams contribute only when the quasiequilibrium state contains finite quasiparticle densities.

The quasiparticle lines are shown in Figs. 7(a) and 7(b) for noninteracting electrons. The physical process can be read off from these diagrams as follows. In the present discussion, we define the term *pair* to mean a conduction electron and valence hole. The first pulse creates a pair, the second annihilates, and the third creates a pair again. Due to the full connectedness of the diagram, this occurs at the same quasimomentum state, and thus represents coherent driving of an electron between the valence and conduction bands. Since the quasiparticle lines are all parallel to the contour, the resulting amplitude is proportional to vacancy of the electron states. In Fig. 7(b), the first pulse is placed on the negative contour, and thus the quasiparticle lines leaving this vertex are anticontour ordered. The result is a diagram proportional to the occupation of electrons. In the solution to the Schrödinger equation, the two diagrams add to form a contribution proportional to the Pauli blocking factor, f_v-f_c. For pulses of finite width, a summation must be performed for different locations of the field lines. In the case of nonoverlapping pulses, the structure of the diagram does not change, and thus only quantitative changes occur. The result is then an expression of the form

$$\int \prod_{j=1,4} d\omega_j e^{-i(\omega_1-\omega_4)t} U_{cv}(\boldsymbol{k}, \omega_1-\omega_2) U_{cv}(\boldsymbol{k}, \omega_3-\omega_4)$$
$$\times U_{vc}(\boldsymbol{k}, \omega_3-\omega_2) A_{\mathrm{Q};cc}(\boldsymbol{k}|\omega_1) A_{\mathrm{Q};vv}(-\boldsymbol{k}|-\omega_2) A_{\mathrm{Q};cc}(\boldsymbol{k}|\omega_3)$$
$$\times A_{\mathrm{Q};hh}(-\boldsymbol{k}|-\omega_4)[1-n_F(\omega_1)][1-n_F(\omega_3)]$$
$$\times[1-n_F(-\omega_2)][1-n_F(-\omega_4)].$$

Here the functions $A_{\mathrm{Q};\zeta\zeta}$ are spectral functions for electrons in band ζ, and n_F is the Fermi distribution function. If pulses are significantly overlapping, then new diagrams would result when the order of field lines changes.

Next we consider the same two diagrams when the Coulomb interaction is present. Figures 7(c) and 7(d) show the case where correlated pairs are generated, but they evolve independently from each other. This diagram would be needed to describe an ideal gas of excitons generated via optical excitation. Note that in both correlation boxes, the vertices connected to the fields occur first. These correlation functions treat the exciton as elementary,[17,18,23] and correspond to the exchange-correlation part of $\langle a^\dagger_v a_c a^\dagger_c a_v \rangle$, where the pair creation is placed to the right of pair annihilation.[24] Similarly, placing the first pulse on the negative contour, as shown in the right-hand side figure, corresponds to the exchange-correlation part of $\langle a^\dagger_c a_v a^\dagger_v a_c \rangle$. On the other hand, placing the second pulse on the positive contour brings the composite nature of the exciton into the process, see Fig. 8. This is so because the third pulse produces a correlated pair that propagates into a state from which the second pulse had removed an electron, but not the valence hole. It can be verified, using a formal expansion over exact eigenstates, that this correlation function is indeed described by a subset of states in the $N-1$ electron Hilbert space of the N-electron system. A symmetrical contribution comes from the states in the $N+1$-electron Hilbert space that results if the second pulse had annihilated a valence hole instead of an electron from a pair. On the other hand, if the outgoing field is the last pulse, then it is easily shown that only the correlation functions of the type $\langle a^\dagger_v a_c a^\dagger_c a_v \rangle$ and $\langle a^\dagger_c a_v a^\dagger_v a_c \rangle$ are involved.

The diagrams introduced above are for two-point correlation functions at $O(U^3)$. We now briefly discuss some diagrams for four-point functions that are $O(U^2)$. Diagrams of this kind are central to the study of multiparticle correlations, and they contribute to the source term $\mathcal{S}^{(2)}_2(14;23)$ of Eq.

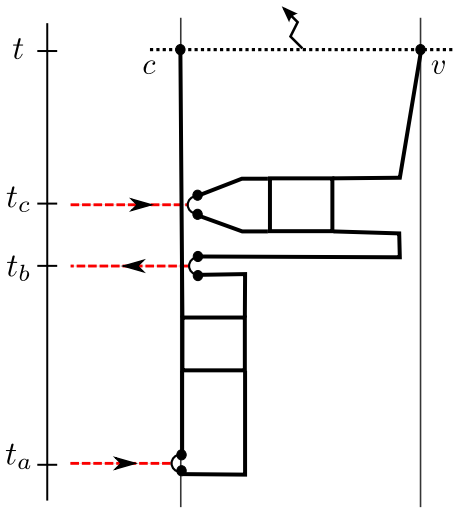

FIG. 8. (Color online) Correlated pair evolution induced by three pulses. The third pulse sees the composite nature of excitons.

(102). With the choice of band and Keldysh indices, many different topologies are possible for $\mathcal{S}_2^{(2)}(14;23)$, of which two are shown in Figs. 9 and 10. Figure 9 shows diagrams with one pulse on each side of the contour. Heuristically speaking, it thus affects both the "bra" and "ket" side of the correlation functions, and leads to coherences among two-particle excited states. In contrast, the diagrams in Fig. 10 contain both pulses on the same side, and they therefore generate coherence between the ground state and a multiparticle excited state—a biexciton state in this case.

In Fig. 9 we show two diagrams contributing to $\mathcal{S}^{(2)}_{2;cvvc}$, which under appropriate excitation frequencies generate Raman coherence between exciton states. The diagram 9(a) couples $\mathfrak{X}^{(2)}_{1;\zeta v;\zeta' c}$ on the "bra" side of the exciton correlation, and directly to the self-consistent field U on the "ket" side, where the interaction blob is taken at quasiequilibrium. Thus this diagram corresponds to the second term of Eq. (102). The diagram 9(a) couples the second pulse to effective interaction, which generates $\Delta I_1^{(2)}$, and corresponds to the second last term of Eq. (102). It can be verified that the first term of Eq. (102) does not contribute to $\mathcal{S}^{(2)}_{2;cvvc}$ in the absence of interband coherence in the quasiequilibrium state. We will discuss these diagrams and their behavior at length in II.

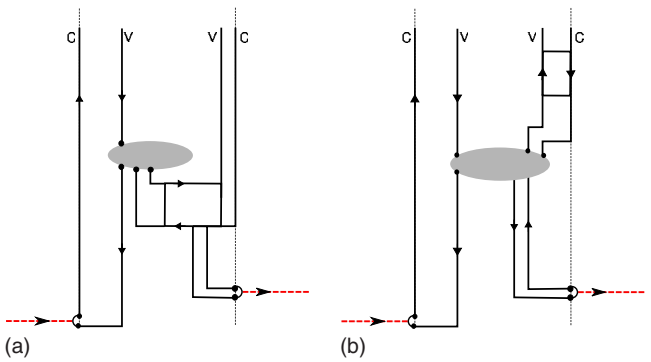

FIG. 9. (Color online) Diagrams for $\mathcal{S}^{(2)}_{2cvvc}(14;23)$, which lead to Raman coherence between two exciton states.

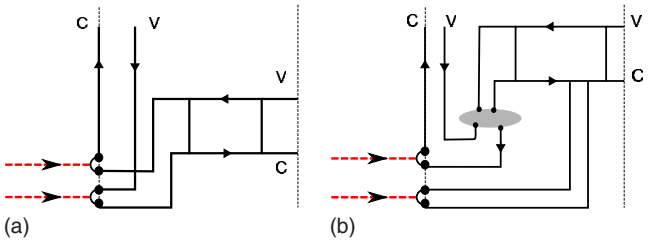

FIG. 10. (Color online) Diagrams contributing to biexciton amplitude $\mathcal{S}^{(2)}_{2cc;vv}(14;23)$.

We now turn to Fig. 10, which shows two contributions to the biexciton source $\mathcal{S}^{(2)}_{2;cc;vv}$. The coherence between a biexciton state and the ground state is a four-point function, a *biexciton amplitude*, which is described by the correlation function $X^{(2)}_{cc;vv}$. The amplitude is given by creation of two conduction electrons and two valence holes, as expected for a coherence between two excitons and the ground state. Its source term is also given by Eq. (102), but where in contrast to Raman coherence, the first term is now a leading order term [shown in Fig. 10(a)]. The term containing $\mathfrak{X}_1^{(2)}$ is shown in Fig. 10(b), where the effective interaction blob is $I^{(2)}_{Qvv;cc}$. These diagrams can be used to build a fully many-body description of the optical generation of biexcitons as a function of pulse parameters, as well as the quasiequilibrium state. Thus we see that the contour diagrams are a useful bookkeeping device that help us understand the relationship of various correlation functions to the pulse sequences and time delays, which constitute experimental input.

C. Signal and two-dimensional spectrum

In this section we discuss the third-order source term, which directly drives the detected signal. We also identify the two-dimensional Fourier spectrum which follows from this signal and can be compared with the one obtained experimentally. The source term is discussed by making several simplifying approximations as our goal is illustration. The calculation of first- and second-order correlations that contribute to this source will be taken up in II, and they are assumed to be known here.

We let the function $\phi_{cv}(\boldsymbol{k},t_1)$ in Eq. (104) be

$$\phi_{cv}(\boldsymbol{k},t) = u_{\boldsymbol{k}} e^{-i\omega t}\delta(t-t_d)\,\delta_{\sigma_1\sigma_2}, \tag{106}$$

where $u_{\boldsymbol{k}}$ is a complex number, and the delta function is an idealization of a pulse with temporal width smaller than the time scale of the dynamics. From Eq. (100), the source driving the correlation $\mathfrak{X}_3^{(1)}(12)$ in its first time argument is

$$\begin{aligned}\mathcal{S}^{(1)}_{3;cv}(12) = {} & G_{\mathrm{Q}}(11')\mathcal{U}_2^{(1)}(1'1'')G_{\mathrm{Q}}(1''2')\mathcal{U}_1^{(1)}(2'2'')G_{\mathrm{Q}}(2''2)\\ & + G_{\mathrm{Q}}(11')\mathcal{U}_1^{(1)}(1'1'')G_{\mathrm{Q}}(1'2')\mathcal{U}_2^{(1)}(2'2'')G_{\mathrm{Q}}(2''2)\\ & + G_{\mathrm{Q}}(11')\mathcal{U}_1^{(1)}(1'1'')G_{\mathrm{Q}}(1''3')\mathcal{U}_1^{(1)}\\ & \times(3'3'')G_{\mathrm{Q}}(3''2')\mathcal{U}_1^{(1)}(2'2'')G_{\mathrm{Q}}(2''2),\end{aligned} \tag{107}$$

where $\mathcal{U}_n^{(1)}$, given by Eq. (98), include the self-energy corrections to U_{cv} beyond Hartree. As expected, the source term contains correlations of the first and second order, and ac-

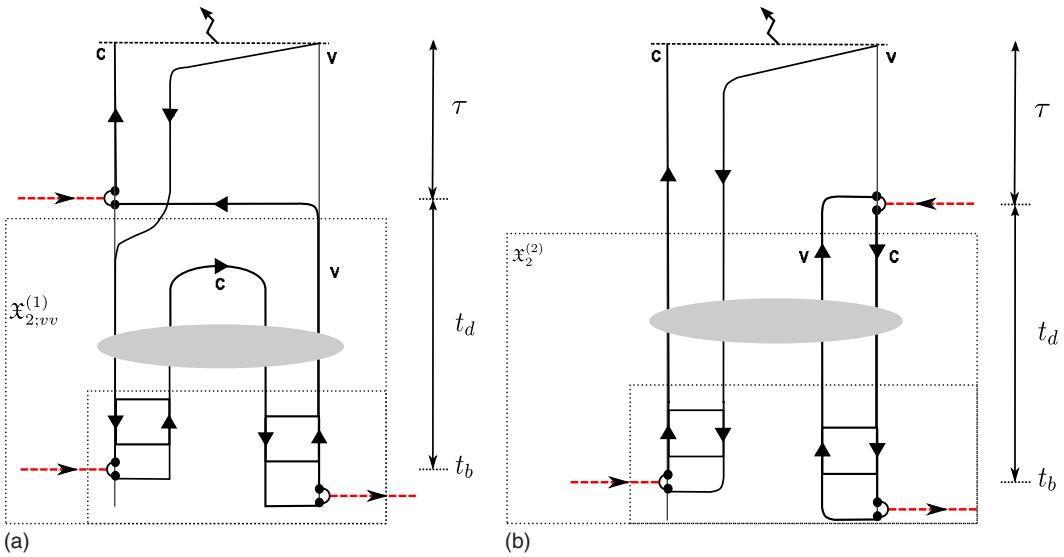

FIG. 11. (Color online) Diagrams for $\mathfrak{X}^{+-}_{3;cv}(tt)$. Intermediate state (before last pulse arrives) is a hole population on the left and exciton on the right and—both these are resonant only at second order in the field in a perturbation expansion.

counts for their interference via quasiparticle propagation between them. This source term has two distinct types of contributions. The first two terms originate from the two-particle correlations arising from (any) two of the pulses, which are linked to the electron-hole correlation from the third pulse by a quasiparticle. That is, the two types of correlations (each of order lower than three) interfere within the phase breaking time of the electron gas. In terms of the BSE of Fig. 4(b), these terms are a sum of all those terms on the right hand side that contain a $X^{(3)}$ block. The third term arises from the rest of the two diagrams on the RHS, which contain products of only four-point functions. This term describes the interference of independent single-particle correlations due to the three pulses. The functions G_{Q} account for propagation as well as memory effects if there is also a time delay between the pulses.

By removing $G_{\mathrm{Q}}(11')$ or $G_{\mathrm{Q}}(2''2)$ from Eq. (107) we obtain the source term for the differential Eq. (68). In general, the dynamical evolution of $\mathfrak{X}^{(1)+-}_{3;cv\boldsymbol{k}}(12)$ must be taken fully into account so as to treat the correlations of each individual pulse on an equal footing. However, $\mathfrak{X}^{(1)+-}_{3;cv\boldsymbol{k}}(12)$ is driven also by the exciton-coherence, unlike the interband polarizations of the first two pulses. Our second paper is devoted to a calculation demonstrating that, under experimentally relevant conditions, the contribution of exciton coherence can last much longer than the interband coherence. In such cases, the dynamical evolution of $\mathfrak{X}^{(1)}_{3}$ has the overall effect of convolving a sharp response function with the above source term. Neglecting all couplings other than the self-coupling, $\Sigma_{\mathrm{Q}}(11')\mathfrak{X}^{(1)}_{3;cv}(1'2)$, which restores the removed G_{Q}, an approximation for the solution is given by the integrated source term. Further corrections can be made on the diagram by allowing interactions between the external vertices 1, and 2. Thus, as alluded to in the previous section, the source diagrams can be used to solve the equations directly. We will see a specific example below.

Figure 11 shows two different contributions to $\mathcal{S}^{(1)}_{3;cv}$. The diagrams show an identical four-point correlation formed by the first two pulses as indicated by the inner-most dashed box. The shaded ellipse in both diagrams stands for a sum of different interaction blobs as identified below. However, the diagrams differ entirely in terms of what it is with which the third pulse interacts. In diagram 11(a) the third pulse interacts with a fully correlated second-order source $\boldsymbol{\mathcal{U}}^{(1)}_{2}$. The line $G^{+-}_{\mathrm{Q}vv}$ directed into the pulse accounts for the effect of hole lifetime in linking this source across a time delay to the pulse. By comparing with Eq. (107), and considering also the case when the interaction blob is absent, the reader may easily verify that this diagram originates from the last two terms. As shown on the diagram, the part of the diagram other than the factor $G_{\mathrm{Q};cc}$ and U_{cv} from the third pulse may be replaced by $\mathfrak{X}^{(1)}_{2;vv}$, or the field-induced hole population. Analogous diagram with $\mathfrak{X}^{(1)}_{2;cc}$ also exists and originates from the first and the last terms of Eq. (107).

These contributions of diagram 11(a) account for the effect of Pauli blocking due to the first two pulses on the driving of the system by the third pulse. This can be seen by writing the source term for the equal time limit for $\mathfrak{X}^{(1)}_{cv}(12)$. We write the source term as a function of the time delays, τ, t_b, and t_d as shown in Fig. 11. It is convenient to switch to the Wigner representation such that a two time function $f(t,t')$ is written as $\tilde{f}[(t+t')/2, t-t']$. Then, letting $S(t_d,\tau,t_b)$ represent $\mathcal{S}^{(1)}_{3}(12)$ as a function of the three variables τ, t_b, and t_d,

$$S(t_d,\tau,t_b) = \int \frac{\mathrm{d}\boldsymbol{k}}{4\pi^2}|u_{\boldsymbol{k}}|^2\left[\tilde{\mathfrak{X}}^{(1)}_{2;vv}\left(\boldsymbol{k}|t_d+t_b+\frac{\tau}{2},\tau\right)\right.$$
$$\left.-\tilde{\mathfrak{X}}^{(1)}_{2;cc}\left(\boldsymbol{k}|t_d+t_b+\frac{\tau}{2},-\tau\right)\right]+S_X(t_d,\tau,t_b), \tag{108}$$

where $t=t_d+t_b+\tau$, and S_X stands for the difference between Eq. (107) and the first term. Thus the Pauli blocking term will map to excitations of the conduction and valence-band populations, and the Fourier transform of this function,

$(t_d,\tau)\rightarrow(\omega,\Omega)$, will naturally contain peaks at $(0,\omega_{vv\boldsymbol{k}})$, and $(0,-\omega_{cc\boldsymbol{k}})$.

Diagram 11(b) contains contributions from entirely different ways of assigning pulses to $\boldsymbol{\mathcal{U}}_j^{(2)}$ depending on the details of effective interaction, and leads to richer possibilities. If the interaction is such that a continuous chain of quasiparticle lines links all three pulses, then this diagram corresponds to the third term Eq. (107). The topology is then like diagram 11(a) and a contribution exists without the interaction as well. When such a continuous chain does not exist, then the diagram corresponds to the first two terms Eq. (107), but now the source $\boldsymbol{\mathcal{U}}_2^{(1)}$ is formed by the first and third pulse. It interacts with the fully correlated source $\boldsymbol{\mathcal{U}}_1^{(2)}$ of the second pulse. The interaction in the latter case is not optional, as it is in diagram 11(a), because its absence would result in a separated form in violation of Rule 6 above. Depending on the topology inside blob, its connection to the first two pulses contributes either a $\Delta I_2^{(2)}$ or the products $G_{\mathcal{Q}}\mathfrak{X}_1^{(1)}\Delta I_1^{(2)}P_{\mathcal{Q}}$, and $G_{\mathcal{Q}}\mathfrak{X}_1^{(1)}\Delta I_{\mathcal{Q}}^{(2)}\mathfrak{X}_1^{(2)}$. All these terms also follow if one performs a formal expansion of Eq. (25) up to second order in the field by making substitutions as in Eq. (34), and in strict application of the formalism they are an application of Rule (e) in the previous section.

As noted above, the resulting expression for the diagram would normally be substituted in the differential equations but it is reasonable to consider an iterative solution instead. We consider building such an iterative solution to Dyson equation by starting from this diagram. The Dyson equation explicitly leads to interactions between the external vertices, 12, and since they correspond to conduction and valence band, respectively, there will be a contribution from the diagrams that form bound exciton states. It is shown in II that there are no interaction free [i.e., $\mathfrak{X}_{1;cc}^{(1)}(13)\mathfrak{X}_{1;vv}^{(1)}(42)$] contributions to this diagram function. From Eq. (25) it then follows that allowing all possible interactions among the four vertices would lead to the function $\mathfrak{X}_{2;cvvc}^{+-\sigma-}(14;23)$, where $\sigma=\pm$, and the 3,4 coordinates are coupled into the third pulse. Thus we obtain the integral form of the excitonic contribution to the solution $\mathfrak{X}_{3;cv\boldsymbol{k}}^{(1)}$,

$$\mathcal{S}_X(11^+)\approx\mathfrak{X}_{2;cvvc}^{+---}(14;1^+4^+)U_{cv}(44^+). \tag{109}$$

Note that the equation is exactly in the form of Eq. (23) when we replace P by $\mathfrak{X}_{2;cvvc}^{(2)}$. Since the third pulse precedes the measurement time, it follows that $\mathfrak{X}_{2;cvvc}^{+---}(14;1^+4^+)=\mathfrak{X}_{2;cvvc}^{+-+-}(14;1^+4^+)$, where the latter can be identified with the exciton correlation (ref. II). Thus the third pulse beats against the two-time exciton correlation. Using the Wigner variables to define a function $\widetilde{\mathcal{P}}$ via

$$\mathfrak{X}_{2;cvvc}^{+-+-}(12;1^+2^+)=\widetilde{\mathcal{P}}_{nm}[(t_1+t_2)/2,t_1-t_2]e^{-i(\omega_n t_1-\omega_m t_2)},$$

we write the approximate solution, Eq. (109), as a function of pulse parameters,

$$\begin{aligned}\mathcal{S}_X(11^+)&\approx S_X(t_d,\tau,t_b)\\&\equiv\theta(\tau)\theta(t_d)\sum_n\varphi_n(\boldsymbol{k})u_m\widetilde{\mathcal{P}}_{nm}\left(t_d+t_b+\frac{\tau}{2},\tau\right)\\&\quad\times e^{-i\omega_{nm}(t_d+t_b)}e^{-i\omega_n\tau/2}.\end{aligned} \tag{110}$$

In Eq. (110) $\theta(\cdot)$ is the step function, $\varphi_n(\boldsymbol{k})$ is the wave function of the exciton state n in momentum space, and u_m is the projection of the transition amplitude onto the exciton state m. Apart from a shift t_b, the source $S(t_d,\tau,t_b)$ maps directly to $\widetilde{\mathcal{P}}$ in this impulse response scheme. Since the evolution of $\mathfrak{X}_{3;cv}$ is linear, this direct mapping extends to that quantity, although convolution with the pulse will make it difficult to relate $\mathfrak{X}_{3;cv}^{(1)}$ and $\widetilde{\mathcal{P}}$ in a straightforward way. We let

$$\widetilde{\mathcal{P}}(\omega,\Omega)=\int_0^\infty d\tau\int_0^{+\infty}dt\widetilde{\mathcal{P}}(t,\tau)e^{i\omega t+i\Omega\tau},$$

which then yields the Fourier transform of the source term,

$$\begin{aligned}S_X(\omega,\Omega)=\sum_{nm}\varphi_n(\boldsymbol{k})u_m\widetilde{\mathcal{P}}_{nm}\left(\omega-\omega_{nm},\Omega-\frac{\omega}{2}-\frac{\omega_n+\omega_m}{2}\right)\\\times e^{-i(\omega-\omega_{nm})t_b}.\end{aligned} \tag{111}$$

The shift ω_{nm} in the first argument represents the fact that it is conjugate to the evolution of the correlation function for a fixed delay. This is also seen from the diagram where t_d maps to the time at which the correlation is two particle. The third pulse directly couples to $\mathcal{P}_{nm}$ from right, and leaves vertices on the left side of the correlation to evolve freely. The evolution of these vertices along the contour produces the factor $e^{-i\omega_n\tau}$ as it evolves. Taking the Fourier transform yields this frequency shift.

Equation (111) is an approximate solution to $\mathfrak{X}_3^{(1)}$, which is a response to the Maxwell field. The radiated field that is detected is given by Eqs. (A11)–(A13), which are written in terms of the expectation value of the current density. In the length gauge the current density operator,

$$\boldsymbol{J}(\boldsymbol{r},t)=\frac{e\hbar}{im}\{\psi^\dagger(\boldsymbol{r},t)\nabla\psi(\boldsymbol{r},t)-[\nabla\psi^\dagger(\boldsymbol{r},t)]\psi(\boldsymbol{r},t)\}, \tag{112}$$

can be rewritten in the Heisenberg picture as

$$\boldsymbol{J}(\boldsymbol{r},t)=-\frac{ie}{\hbar}\psi^\dagger(\boldsymbol{r},t)[\mathcal{H}(t),\hat{\boldsymbol{r}}]\psi(\boldsymbol{r},t), \tag{113}$$

due to the commutativity of Coulomb interaction with the position operator, $\hat{\boldsymbol{r}}$. The desired expectation value from the above equation is then

$$\langle\boldsymbol{J}\rangle=-\frac{e}{\hbar}\mathrm{Tr}\{[\mathcal{H}(t),\hat{\boldsymbol{r}}]G(11^+)\}, \tag{114}$$

where we have switched to the Schrödinger picture for operators inside the trace. The $O(U^3)$ contribution to the current density within the two-band model employed here is

$$\begin{aligned}\langle\boldsymbol{J}^{(3)}(\boldsymbol{q},t)\rangle=-e\,\delta(\boldsymbol{q}-\boldsymbol{k}_1+\boldsymbol{k}_2-\boldsymbol{k}_3)\\\times\int\frac{d\boldsymbol{k}}{4\pi^2}\{\omega_{cv}(\boldsymbol{k})\hat{\boldsymbol{r}}_{vc}(\boldsymbol{k})\mathfrak{X}_{3;cv}^{(1)}(\boldsymbol{k}t;\boldsymbol{k}t^+)+\text{c.c.}\},\end{aligned} \tag{115}$$

where $\boldsymbol{k}_i$ are wave vectors of the three optical fields. The

summation in Eq. (115) is essentially given by S_X Eq. (111) apart from the additional factor of kinetic energy of the electron and hole. This expression is substituted into Eq. (A11) to obtain the TDFS signal in the far field.

V. CONCLUSION

We have developed a framework suitable for applications to multipulse optical excitations of semiconductors based on nonequilibrium Green functions. In particular, it specifically addresses multidimensional Fourier spectroscopy experiments. A calculation begins with a model of the many-body system in a quasiequilibrium state, where the important quasiparticle species and the scattering processes are taken into account by vertex corrections to the self-energy. The formalism then applies functional differentiation to determine variations in the single-particle Green function up to third order, by computing the respective variations in self-energy.

This straightforward and physically motivated method requires a sufficiently complex machinery to be stated in an explicit form. We have discussed the challenges posed by the hierarchy of many-body correlation functions, and the form in which it appears in the current context. A possible truncation method was discussed and applied; it is analogous to the use of noninteracting two-particle correlation functions in the *GW* approximation. However, the truncation used here is a self-consistent solution for up to n-order correlation functions that includes the effects of all scattering channels involving n particles. This allows for a consistent treatment of decoherence processes, since all scattering processes at a given level of scattering are present by construction. Although we did not discuss the general treatment of this explicitly, we showed the explicit dynamical maps for up to four-point functions. This already includes decoherence effects of all two-particle interactions on, for instance, the exciton and biexciton correlation functions. These general equations, when specialized to particular cases, produce effective models that are appropriate to study decoherence by way of many-body correlation functions. A first set of calculations of these effects is presented in the accompanying publication (II).

The basic structure of the formalism consists of a set of dynamical variables that are deviations of correlation functions of the quasiequilibrium state. These deviations then evolve according to linear dynamical maps, which form one part of driven differential equations. The dynamical maps are given by kernels, which correspond to correlation functions and screened interactions of the quasiequilibrium. Thus a consistent way of including necessary resummations is built into the formalism.

The second part of these equations are the source terms, the simplest of which is just the optical field. At a given order in the field, deviations of all lower orders combine to form local field corrections to this source term, and eventually form the only link between the observed signal and multiparticle states in the system. We have identified and discussed the physical interpretation of these terms.

The source terms are also conveniently described by diagrams on the Keldysh contour, which turn out to be a natural extension of the double-sided Feynman diagrams used in more phenomenological treatments. While keeping the same bookkeeping of optical excitations, they allow for a description of the interaction processes as well. Their characterization of source terms is completed by a set of rules that translate a diagram to a mathematical expression for a source, and vice versa. The arrangement of three pulses, and physical parameters of the quasiequilibrium state such as densities, temperatures, and chemical potentials, can then be combined to identify the dominant sources. By the same token, they can be used to identify appropriate pulse sequences for suppressing or enhancing certain superpositions. We mentioned only simple examples of this, as the detailed investigation must be done case by case.

The full solution to the above set of equations is not numerically feasible at present. However, the purpose of this framework is to act as a starting point to model a particular experimental situation, with a solvable approximation to the multiparticle correlation functions. Within simple parametrization of the screened interaction, which is a reasonable expansion parameter as opposed to the bare interaction, the kernels of the dynamical maps can be constructed approximately. We show in II that it leads to a two-time generalization of a Lindblad map for exciton correlations, where the kernel to the lowest order is proportional to interaction and density-density correlation of the quasiequilibrium state.

The class of problems where this method is the most appropriate is optically induced dynamics of a multiparticle system that contains finite density of quasiparticles. Thus within the field of semiconductor optics, doped (optically or impurity) quantum wells constitute an obvious system for testing this theory. Here the decoherence phenomenon occurs in a new regime, where system and bath particles are indistinguishable. The framework is also a valuable background against which to develop phenomenological models, and provides a firm grounding of these models in a microscopic description.

ACKNOWLEDGMENTS

This work was supported by the Natural Sciences and Engineering Research Council (NSERC) of Canada. K.S.V. acknowledges support from NSERC. We thank S. T. Cundiff and members of his research group for many helpful discussions.

APPENDIX A: ELECTRODYNAMICS

If we take Fourier transforms with respect to both time and the x and y coordinates, writing for example

$$\boldsymbol{E}_d(\boldsymbol{r},t) = \int \frac{d\omega}{2\pi} \boldsymbol{E}_d(\boldsymbol{r},\omega) e^{-i\omega t},$$

where

$$\boldsymbol{E}_d(\boldsymbol{r},\omega) = \int \frac{d\boldsymbol{k}}{(2\pi)^2} \boldsymbol{E}_d(\boldsymbol{k},z;\omega) e^{i\boldsymbol{k}\cdot\boldsymbol{R}}$$

with $\boldsymbol{k}=(k_x,k_y)$ and $\boldsymbol{R}=(x,y)$, we have

$$\boldsymbol{E}_d(\boldsymbol{k},z;\omega) = i\omega^{-1}\int \mathcal{G}(\boldsymbol{k},z-z';\omega)\langle \boldsymbol{J}(\boldsymbol{k},z';\omega)\rangle dz', \tag{A1}$$

where

$$\mathcal{G}(\boldsymbol{k},z-z';\omega) = \frac{i\tilde{\omega}^2}{2\epsilon_0 w}\theta(z-z')(\hat{\boldsymbol{s}}\hat{\boldsymbol{s}}+\hat{\boldsymbol{p}}_+\hat{\boldsymbol{p}}_+)e^{iw(z-z')} + \frac{i\tilde{\omega}^2}{2\epsilon_0 w}\theta(z'-z)(\hat{\boldsymbol{s}}\hat{\boldsymbol{s}}+\hat{\boldsymbol{p}}_-\hat{\boldsymbol{p}}_-) \times e^{-iw(z-z')} - \frac{\hat{\boldsymbol{z}}\hat{\boldsymbol{z}}}{\epsilon_0\varepsilon}\delta(z-z'), \tag{A2}$$

with ϵ_0 the permittivity of free space, $\tilde{\omega}=\omega/c$, $w=\sqrt{\tilde{\omega}^2\varepsilon-k^2}$ (Im $w\geq 0$, with Re $w\geq 0$ if Im $w=0$), where $k=|\boldsymbol{k}|$, $\theta(z)$ is the step function [$\theta(z)=0$ or 1 as $z<0$ or $z>0$] and the unit vectors $\hat{\boldsymbol{s}}$ and $\hat{\boldsymbol{p}}_\pm$ are given by

$$\hat{\boldsymbol{s}} \equiv \hat{\boldsymbol{k}}\times\hat{\boldsymbol{z}},$$

$$\hat{\boldsymbol{p}}_\pm \equiv \frac{k\hat{\boldsymbol{z}} \mp w\hat{\boldsymbol{k}}}{\tilde{\omega}\sqrt{\varepsilon}},$$

where $\hat{\boldsymbol{k}}=\boldsymbol{k}/k$. This follows directly from the solution of the Maxwell equations.[25] Far from the source but within the semiconductor, say for $z>0$, if we fix $\hat{\boldsymbol{r}}$ and let $r\to\infty$ we find,

$$\boldsymbol{E}_d(\hat{\boldsymbol{r}}r,\omega) \sim \frac{i\mu_0\omega}{4\pi}\frac{e^{i\tilde{\omega}\sqrt{\varepsilon}r}}{r}\boldsymbol{\gamma}\cdot\int\langle \boldsymbol{J}(\boldsymbol{k}_o,z';\omega)\rangle dz' \tag{A3}$$

where μ_0 is the permeability of free space, $\boldsymbol{k}_o=\tilde{\omega}\sqrt{\varepsilon}[\hat{\boldsymbol{r}}-\hat{\boldsymbol{z}}(\hat{\boldsymbol{z}}\cdot\hat{\boldsymbol{r}})]$, and $\boldsymbol{\gamma}=(\hat{\boldsymbol{s}}\hat{\boldsymbol{s}}+\hat{\boldsymbol{p}}_+\hat{\boldsymbol{p}}_+)$ evaluated at $\boldsymbol{k}=\boldsymbol{k}_o$.[26] Alternatively, if the quantum well is close to a semiconductor interface with air or another material, the Fresnel coefficients can be applied to the s- and p-polarized components of the field Eq. (A1) to find the field outside the semiconductor, and then a corresponding asymptotic result can be deduced. Hence once $\langle \boldsymbol{J}(\boldsymbol{r},t)\rangle$ is determined the radiation signal is easily found. We address the problem of calculating $\langle \boldsymbol{J}(\boldsymbol{r},t)\rangle$ from a many-body framework using nonequilibrium Green functions.

In the absence of any perturbing field, the standard Hamiltonian of many-body physics is Eq. (2) with $\boldsymbol{A}_{nom}(t)=0$. The simplest way to generalize that Hamiltonian to include the effect of an incident field $\boldsymbol{E}_{inc}(\boldsymbol{r},t)$ on the system, when that incident field is treated classically, is to describe the field by potentials and include them as time dependent terms in the Hamiltonian. Since we are dealing with pulses of light, the simplest gauge is the so-called radiation gauge, where no scalar potential is introduced for $\boldsymbol{E}_{inc}(\boldsymbol{r},t)$ but we write simply $\boldsymbol{E}_{inc}(\boldsymbol{r},t)=-\partial\boldsymbol{A}_{inc}(\boldsymbol{r},t)/\partial t$, describing both magnetic and electric fields in terms of only a vector potential. The inclusion of this vector potential in the Hamiltonian leads to

$$\mathcal{H}(t) = \frac{1}{2m}\int\left[\left(\frac{\hbar}{i}\nabla - e\boldsymbol{A}_{inc}(\boldsymbol{r},t)\right)\psi(\boldsymbol{r})\right]^\dagger \times\left[\left(\frac{\hbar}{i}\nabla - e\boldsymbol{A}_{inc}(\boldsymbol{r},t)\right)\psi(\boldsymbol{r})\right]d\boldsymbol{r} + \int v_0(\boldsymbol{r})\psi^\dagger(\boldsymbol{r})\psi(\boldsymbol{r})d\boldsymbol{r} + \int\psi^\dagger(\boldsymbol{r})\psi^\dagger(\boldsymbol{r}')v(\boldsymbol{r}-\boldsymbol{r}')\psi(\boldsymbol{r}')\psi(\boldsymbol{r})d\boldsymbol{r}d\boldsymbol{r}'. \tag{A4}$$

In describing the response to the incident field, however, it would be worrying to neglect the transverse component of the field due to the electrons, even if that component can be neglected in equilibrium calculations. One reason is that, since the incident field is a transverse field, it would seem natural to take into account the transverse field from the driven charge-current densities themselves. A second reason is more specific: It is through the interaction of the charge-current density with its own transverse field (the so-called "radiation reaction") that the system responds to the fact that it is radiating energy to infinity.[27] Hence taking into account the effects of the transverse field of the charge-current densities on those densities themselves is essential for maintaining energy conservation.

At the level of the semiclassical description used here, the field radiated to infinity follows from the expectation value of the current density (A1). Thus in calculating the dynamics of the charge-current densities it is appropriate to include the expectation value of the transverse field generated by the charge-current densities as an additional driving field,

$$\boldsymbol{E}_T(\boldsymbol{k},z;\omega) = i\omega^{-1}\int\mathcal{G}_T(\boldsymbol{k},z-z';\omega)\langle \boldsymbol{J}(\boldsymbol{k},z';\omega)\rangle,$$

where

$$\mathcal{G}_T(\boldsymbol{k},z;\omega) = \mathcal{G}(\boldsymbol{k},z;\omega) - \mathcal{G}_L(\boldsymbol{k},z;\omega), \tag{A5}$$

with $\mathcal{G}_L(\boldsymbol{k},z;\omega)=\lim_{\tilde{\omega}/k\to 0}\mathcal{G}(\boldsymbol{k},z;\omega)$. Again using the radiation gauge by writing $\boldsymbol{E}_T(\boldsymbol{r},t)=-\partial\boldsymbol{A}_T(\boldsymbol{r},t)/\partial t$, we introduce an effective vector potential

$$\boldsymbol{A}_{eff}(\boldsymbol{r},t) = \boldsymbol{A}_{inc}(\boldsymbol{r},t) + \boldsymbol{A}_T(\boldsymbol{r},t), \tag{A6}$$

and take as our time-dependent Hamiltonian

$$\mathcal{H}(t) = \frac{1}{2m}\int\left[\left(\frac{\hbar}{i}\nabla - e\boldsymbol{A}_{eff}(\boldsymbol{r},t)\right)\psi(\boldsymbol{r})\right]^\dagger \times\left[\left(\frac{\hbar}{i}\nabla - e\boldsymbol{A}_{eff}(\boldsymbol{r},t)\right)\psi(\boldsymbol{r})\right]d\boldsymbol{r} + \int v_0(\boldsymbol{r})\psi^\dagger(\boldsymbol{r})\psi(\boldsymbol{r})d\boldsymbol{r} + \int\psi^\dagger(\boldsymbol{r})\psi^\dagger(\boldsymbol{r}')v(\boldsymbol{r}-\boldsymbol{r}')\psi(\boldsymbol{r}')\psi(\boldsymbol{r})d\boldsymbol{r}d\boldsymbol{r}'. \tag{A7}$$

The strategy is to use the Hamiltonian (A7) to solve for $\langle\rho(\boldsymbol{r},t)\rangle$ and $\langle \boldsymbol{J}(\boldsymbol{r},t)\rangle$ in terms of $\boldsymbol{A}_{eff}(\boldsymbol{r},t)$; then using Eq. (A6) and writing $\boldsymbol{A}_T(\boldsymbol{r},t)$ in terms of $\langle \boldsymbol{J}(\boldsymbol{r},t)\rangle$, one can in principle find $\langle\rho(\boldsymbol{r},t)\rangle$ and $\langle \boldsymbol{J}(\boldsymbol{r},t)\rangle$ self-consistently in terms of $\boldsymbol{A}_{inc}(\boldsymbol{r},t)$ and hence in terms of $\boldsymbol{E}_{inc}(\boldsymbol{r},t)$. Using Eq. (A1) the signal field generated is then identified.

In practice the problem simplifies because of the different length scales involved. The variation of $\boldsymbol{E}_{inc}(\boldsymbol{r},t)$ [and thus $\boldsymbol{A}_{inc}(\boldsymbol{r},t)$] is on the order of the wavelength of light λ, which is much greater than the thickness of the quantum well, typical exciton radii, and of course the lattice constant $\mathfrak{a}$. To identify the length scale over which $\boldsymbol{E}_T(\boldsymbol{r},t)$ varies, note that the expectation value $\langle \boldsymbol{J}(\boldsymbol{k},z;\omega)\rangle$ will have $\boldsymbol{k}$ components with k on the order of λ^{-1} and on the order of $\mathfrak{a}^{-1} \gg \lambda^{-1}$. For large $k/\tilde{\omega}$ the transverse component of the electric field becomes negligible, as can be seen from evaluating the terms in Eq. (A5); and in any case the large transverse components $k \simeq \mathfrak{a}^{-1} \gg \tilde{\omega}\sqrt{\varepsilon}$ lead to evanescent fields that do not carry energy to infinity, and hence are not responsible for radiation reaction and not of primary interest. Thus we need only consider components $k \simeq \lambda^{-1}$, and for such components we find

$$\mathcal{G}_T(\boldsymbol{k},z-z';\omega) \simeq \mathcal{G}_T(\boldsymbol{k};\omega) \equiv \frac{i}{2\epsilon_0}\left[\frac{\tilde{\omega}^2}{w}\hat{\boldsymbol{s}}\hat{\boldsymbol{s}} + \left(\frac{k^2}{\varepsilon w} + \frac{ik}{\varepsilon}\right)\hat{\boldsymbol{z}}\hat{\boldsymbol{z}} + \left(\frac{w-ik}{\varepsilon}\right)\hat{\boldsymbol{k}}\hat{\boldsymbol{k}}\right] \quad \text{for} \quad |z-z'| \ll \lambda. \tag{A8}$$

from Eq. (A5). So $\boldsymbol{E}_T(\boldsymbol{r},t)$, like $\boldsymbol{E}_{inc}(\boldsymbol{r},t)$, is essentially uniform over the quantum well and varies slowly, over a range on the order of λ, as x and y vary.

This range is larger than the typical exciton radii that will characterize the correlation lengths of the electron field operators. This suggests the following strategy: (a) To determine the response in the neighborhood of each $(x_o y_o)$, replace $\boldsymbol{E}_{eff}(\boldsymbol{r},t)$ and hence $\boldsymbol{A}_{eff}(\boldsymbol{r},t)$ by a nominal uniform effective field and potential $\boldsymbol{E}_{nom}(t)$ and $\boldsymbol{A}_{nom}(t)$, but with values equal to the actual $\boldsymbol{E}_{eff}(x_o,y_o,0,t)$ and $\boldsymbol{A}_{eff}(x_o,y_o,0,t)$, and then (b) solve for the $\langle \rho(\boldsymbol{r},t)\rangle$ and $\langle \boldsymbol{J}(\boldsymbol{r},t)\rangle$ that follow from the Hamiltonian (2), and call them $\langle \rho^o(\boldsymbol{r},t)\rangle$ and $\langle \boldsymbol{J}^o(\boldsymbol{r},t)\rangle$. As functions of x and y these will be uniform except for variations on the order of the lattice constant. We denote the components that are uniform over x and y by $\langle \bar{\rho}(\boldsymbol{r},t)\rangle$ and $\langle \bar{\boldsymbol{J}}(\boldsymbol{r},t)\rangle$; they are functionals of $\boldsymbol{A}_{nom}(t)$ and hence of $\boldsymbol{E}_{nom}(t)$,

$$\langle \bar{\rho}(\boldsymbol{r},t)\rangle = \mathcal{F}_\rho[\boldsymbol{E}_{nom}(t)],$$

$$\langle \bar{\boldsymbol{J}}(\boldsymbol{r},t)\rangle = \mathcal{F}_{\boldsymbol{J}}[\boldsymbol{E}_{nom}(t)].$$

(c) Finally, adopting these expressions as a good characterization of the actual response of the system in the neighborhood of each $(x_o y_o)$, we take

$$\langle \bar{\rho}_{eff}(\boldsymbol{r},t)\rangle = \mathcal{F}_\rho[\boldsymbol{E}_{eff}(x,y,0,t)],$$

$$\langle \bar{\boldsymbol{J}}_{eff}(\boldsymbol{r},t)\rangle = \mathcal{F}_{\boldsymbol{J}}[\boldsymbol{E}_{eff}(x,y,0,t)], \tag{A9}$$

where $\langle \bar{\rho}_{eff}(\boldsymbol{r},t)\rangle$ and $\langle \bar{\boldsymbol{J}}_{eff}(\boldsymbol{r},t)\rangle$ denote the actual $\langle \rho(\boldsymbol{r},t)\rangle$ and $\langle \boldsymbol{J}(\boldsymbol{r},t)\rangle$, within our approximations, when averaged in the xy plane over distances on the order of the lattice constant. This allows for $\langle \bar{\rho}_{eff}(\boldsymbol{r},t)\rangle$ and $\langle \bar{\boldsymbol{J}}_{eff}(\boldsymbol{r},t)\rangle$ to adiabatically follow the slow variation of the effective field as it varies of distances on the order of λ in the plane of the quantum well.

The averaging involved in constructing $\langle \bar{\rho}_{eff}(\boldsymbol{k},z;\omega)\rangle$ and $\langle \bar{\boldsymbol{J}}_{eff}(\boldsymbol{k},z;\omega)\rangle$ means that there will be components $\boldsymbol{k}$ in $\langle \rho(\boldsymbol{k},z;\omega)\rangle$ and $\langle \boldsymbol{J}(\boldsymbol{k},z;\omega)\rangle$ that will be lost in $\langle \bar{\rho}(\boldsymbol{k},z;\omega)\rangle$ and $\langle \boldsymbol{J}(\mathbf{k},z;\omega)\rangle$. But since those components will have $k \simeq \mathfrak{a}^{-1}$ they will not contribute to the signal field that can propagate to infinity, and in place of Eqs. (A1) and (A3) we can write, respectively

$$\boldsymbol{E}_d(\boldsymbol{k},z;\omega) = i\omega^{-1}\int \mathcal{G}(\boldsymbol{k},z-z';\omega)\langle \bar{\boldsymbol{J}}_{eff}(\boldsymbol{k},z';\omega)\rangle dz' \tag{A10}$$

and

$$\boldsymbol{E}_d(\hat{\boldsymbol{r}}r,\omega) \sim \frac{i\mu_0\omega}{4\pi}\frac{e^{i\tilde{\omega}\sqrt{\varepsilon}r}}{r}\boldsymbol{\gamma}\cdot\int \langle \bar{\boldsymbol{J}}_{eff}(\boldsymbol{k}_o,z';\omega)\rangle dz' \tag{A11}$$

for evaluating the signal field away from the quantum well. Note that even a few lattice spacings away from the quantum well Eq. (A10) will essentially agree with Eq. (A1). In Eq. (A9) we put

$$\boldsymbol{E}_{eff}(x,y,0,t) = \boldsymbol{E}_{inc}(x,y,0,t) + \boldsymbol{E}_T(x,y,0,t), \tag{A12}$$

[cf. Eq. (A6)], and using Eq. (A8) we have

$$\boldsymbol{E}_T(\boldsymbol{k},0;\omega) = i\omega^{-1}\mathcal{G}_T(\boldsymbol{k};\omega)\cdot\mathcal{J}(\boldsymbol{k};\omega), \tag{A13}$$

where

$$\mathcal{J}(\boldsymbol{k};\omega) = \int \langle \bar{\boldsymbol{J}}_{eff}(\boldsymbol{k},z';\omega)\rangle dz'.$$

Since $\boldsymbol{E}_T(\boldsymbol{k},0;\omega)$ in fact only involves the total integral over z of $\langle \bar{\boldsymbol{J}}_{eff}(\boldsymbol{k},z;\omega)\rangle$, the consistent solution of Eqs. (A9), (A12), and (A13) is feasible, at least within a perturbation scheme.

This approach can be generalized to deal with multiwell structures, if effects such as Coulomb drag are neglected. That is, while fully taking into account the many-body effects within each well, we assume that we can treat the interaction between wells at the mean field level, for both the longitudinal and transverse components of the electromagnetic field. Then, if the wells are all identical with their centers located by z_m, we take

$$\langle \bar{\rho}_{eff}(x,y,z+z_m,t)\rangle = \mathcal{F}_\rho[\boldsymbol{E}_{eff}(x,y,z_m,t)],$$

$$\langle \bar{\boldsymbol{J}}_{eff}(x,y,z+z_m,t)\rangle = \mathcal{F}_{\boldsymbol{J}}[\boldsymbol{E}_{eff}(x,y,z_m,t)], \tag{A14}$$

where $\mathcal{F}_\rho$ and $\mathcal{F}_{\boldsymbol{J}}$ are the functionals introduced above for a single quantum well [cf. Eq. (A9)]; the effective field at each well is then

$$\boldsymbol{E}_{eff}(x,y,z_m,t) = \boldsymbol{E}_{inc}(x,y,z_m,t) + \boldsymbol{E}_{wells}(x,y,z_m,t) \tag{A15}$$

[cf. Eq. (A12)], where now

$$\boldsymbol{E}_{wells}(\boldsymbol{k},z_m;\omega) = i\omega^{-1}\mathcal{G}_T(\boldsymbol{k};\omega)\cdot\mathcal{J}_m(\boldsymbol{k};\omega) + i\omega^{-1}\sum_{m'\neq m}\mathcal{G}(\boldsymbol{k},z_m-z_{m'};\omega)\cdot\mathcal{J}_{m'}(\boldsymbol{k};\omega), \tag{A16}$$

[cf. Eq. (A13)] with

$$\mathcal{J}_m(\boldsymbol{k};\omega) = \int_{well\ m}\langle\bar{\boldsymbol{J}}_{eff}(\boldsymbol{k},z';\omega)\rangle dz'. \tag{A17}$$

The full $\mathcal{G}$ appears in Eq. (A16) for $m'\neq m$ because it carries both the transverse and the longitudinal field from well m' and the position of well m. The integral originally appearing in Eq. (A1) has been replaced by the sum in Eq. (A16) because, except for the Dirac delta function term in Eq. (A2) that does not contribute if z and z' are in different wells, $\mathcal{G}(\boldsymbol{k},z-z';\omega)$ varies slowly as z and z' vary over a quantum well for the $k\simeq\lambda^{-1}$ that appear. This also allows us to write our signal field as

$$\boldsymbol{E}_d(\boldsymbol{k},z;\omega) = i\omega^{-1}\sum_m \mathcal{G}(\boldsymbol{k},z-z_m;\omega)\cdot\mathcal{J}_m(\boldsymbol{k};\omega) \tag{A18}$$

for planes z at least a few lattice constants away from any quantum well.

Equations (A14)–(A18) allow us to determine the signal field and its dependence on the incident field $\boldsymbol{E}_{inc}(\boldsymbol{r},t)$ in a TDFS experiment once the functionals $\mathcal{F}_\rho$ and $\mathcal{F}_{\boldsymbol{J}}$ are identified. That identification is the main task of the text of this paper.

APPENDIX B: EFFECTIVE TWO-PARTICLE INTERACTION: DETAILS

An explicit expression for $I^{(2)}$ follows from the functional derivative of Eq. (31) with respect to G, yielding

$$I^{(2)}(14;23) = i\int W(15;5'3)\Gamma(45';25) + i\int\frac{\delta W(15;5'6)}{\delta G(34)}G(11')\Gamma(1'6;25) + i\int W(15;5'6)G(61')\frac{\delta\Gamma(1'6;25)}{\delta G(34)}.$$

From the formal solution of Eq. (27) we find

$$\frac{\delta W(14;23)}{\delta G(3'4')} = -iW(15;63)\frac{\delta P(68;57)}{\delta G(3'4')}W(74;28)$$
$$= -iW(15;63)\{G(5'5)\Gamma(68;5'7)+G(66')\Gamma(6'8;57)\}W(74;28) - iW(15;63)\{\Gamma(68;57')G(7'7) + \Gamma(68';57)G(8'8)\}W(74;28) - iW(15;63)\left\{G(5'5)G(66')\frac{\delta T(6'8';5'7')}{\delta G(3'4')}G(7'7)G(8'8)\right\}W(74;28),$$

and substituting this in the equation for $I^{(2)}$ yields

$$I^{(2)}(14;23) = i\int W(15;5'1')\Gamma(1'5';25) + i\int W(14;61')G(11'')G(66')T(1''6';23) + i\int W(15;31')G(11'')G(5'5)T(1''4;25')$$
$$+\int W(1\tilde{5};61')\{G(\tilde{5}'\tilde{5})\Gamma(68;\tilde{5}'7)+G(66')\Gamma(6'8;\tilde{5}7)\}W(75;5'8)G(1'1'')\Gamma(1''5';25)$$
$$+\int W(1\tilde{5};61')\{\Gamma(68;\tilde{5}7')G(7'7)+\Gamma(68';\tilde{5}7)G(8'8)\}W(75;5'8)G(1'1'')\Gamma(1''5';25)$$
$$+\int W(1\tilde{5};61')\left\{G(\tilde{5}'\tilde{5})G(66')\frac{\delta T(6'8';\tilde{5}'7')}{\delta G(3'4')}G(7'7)G(8'8)\right\}W(75;5'8)G(1'1'')\Gamma(1''5';25)$$
$$+i\int W(15;61')G(11'')G(5'5)G(66')\frac{\delta T(1''6';25')}{\delta G(34)}.$$

The equation is understood most clearly in the form of diagrams shown in Section II B.

APPENDIX C: DERIVATION OF INTEGRAL BETHE-SALPETER EQUATIONS

We start with the Dyson equation

$$G = G_0 + G_0 \tilde{\Sigma} G,$$

$$\tilde{\Sigma} \equiv U_{\mathrm{Q}} + U + \Sigma.$$

Using the identity $\delta G = -G\delta G^{-1} G$, where $G^{-1} = G_0^{-1} - \tilde{\Sigma}$, the three functional derivatives of G follow:

$$X^{(2)}(1a';2a) = \frac{\delta G(12)}{\delta U_{aa'}} = G(11') \frac{\delta \tilde{\Sigma}(1'2')}{\delta U_{aa'}} G(2'2) \tag{C1}$$

$$\begin{aligned} X^{(3)}(1b'a';2ba) &= \frac{\delta}{\delta U_{bb'}} \frac{\delta G(12)}{\delta U_{aa'}} \\ &= \left[\frac{\delta G(11')}{\delta U_{bb'}} G(2'2) + G(11') \frac{\delta G(2'2)}{\delta U_{bb'}} \right] \frac{\delta \tilde{\Sigma}(1'2')}{\delta U_{aa'}} \\ &\quad + G(11') G(2'2) \frac{\delta^2 \tilde{\Sigma}(1'2')}{\delta U_{bb'} \delta U_{aa'}}, \end{aligned} \tag{C2}$$

$$\begin{aligned} X^{(4)}(1c'b'a';2cba) &= \frac{\delta^3 G(12)}{\delta U_{cc'} \delta U_{bb'} \delta U_{aa'}} \\ &= G(11') G(2'2) \frac{\delta^3 \tilde{\Sigma}(1'2')}{\delta U_{cc'} \delta U_{bb'} \delta U_{aa'}} \left[\frac{\delta G(11')}{\delta U_{bb'}} \frac{\delta G(2'2)}{\delta U_{cc'}} \right. \\ &\quad \left. + \frac{\delta G(11')}{\delta U_{cc'}} \frac{\delta G(2'2)}{\delta U_{bb'}} \right] \frac{\delta \tilde{\Sigma}(1'2')}{\delta U_{aa'}} \\ &\quad + \left[\frac{\delta G(11')}{\delta U_{cc'}} G(2'2) + G(11') \frac{\delta G(2'2)}{\delta U_{cc'}} \right] \frac{\delta^2 \tilde{\Sigma}(1'2')}{\delta U_{bb'} \delta U_{aa'}} \\ &\quad + \left[\frac{\delta G(11')}{\delta U_{bb'}} G(2'2) + G(11') \frac{\delta G(2'2)}{\delta U_{bb'}} \right] \frac{\delta^2 \tilde{\Sigma}(1'2')}{\delta U_{cc'} \delta U_{aa'}} \\ &\quad + \left[\frac{\delta^2 G(11')}{\delta U_{cc'} \delta U_{bb'}} G(2'2) + G(11') \frac{\delta^2 G(2'2)}{\delta U_{cc'} \delta U_{bb'}} \right] \\ &\quad \times \frac{\delta \tilde{\Sigma}(1'2')}{\delta U_{aa'}}. \end{aligned} \tag{C3}$$

Next we obtain expressions for the first three derivatives of the self-energy,

$$\frac{\delta \tilde{\Sigma}(12)}{\delta U_{aa'}} = \delta(1a)\delta(2'a') + \frac{\delta \Sigma(12)}{\delta G(34)} \frac{\delta G(34)}{\delta U_{aa'}}, \tag{C4}$$

$$\begin{aligned} \frac{\delta^2 \tilde{\Sigma}(12)}{\delta U_{bb'} \delta U_{aa'}} &= \frac{\delta \Sigma(12)}{\delta G(34)} \frac{\delta^2 G(34)}{\delta U_{bb'} \delta U_{aa'}} \\ &\quad + \frac{\delta^2 \Sigma(12)}{\delta G(56) \delta G(34)} \frac{\delta G(56)}{\delta U_{bb'}} \frac{\delta G(34)}{\delta U_{aa'}}, \end{aligned} \tag{C5}$$

$$\begin{aligned} \frac{\delta^3 \tilde{\Sigma}(12)}{\delta U_{cc'} \delta U_{bb'} \delta U_{aa'}} &= \frac{\delta^3 \Sigma(12)}{\delta G(78) \delta G(56) \delta G(34)} \frac{\delta G(78)}{\delta U_{cc'}} \frac{\delta G(56)}{\delta U_{bb'}} \frac{\delta G(34)}{\delta U_{aa'}} \\ &\quad + \frac{\delta \Sigma(12)}{\delta G(34)} \frac{\delta^3 G(34)}{\delta U_{cc'} \delta U_{bb'} \delta U_{aa'}} \\ &\quad + \frac{\delta^2 \Sigma(12)}{\delta G(56) \delta G(34)} \left[\frac{\delta G(56)}{\delta U_{cc'}} \frac{\delta^2 G(34)}{\delta U_{bb'} \delta U_{aa'}} \right. \\ &\quad \left. + \frac{\delta G(34)}{\delta U_{aa'}} \frac{\delta^2 G(56)}{\delta U_{cc'} \delta U_{bb'}} + \frac{\delta G(56)}{\delta U_{bb'}} \frac{\delta^2 G(34)}{\delta U_{cc'} \delta U_{aa'}} \right]. \end{aligned} \tag{C6}$$

These substituted in Eqs. (C1) and (C2) result in equations written entirely in terms of G and effective interaction constructed by removing G from the self-energy graphs. The effective interaction is defined in Eq. (44).

APPENDIX D: TRANSFORMING BETWEEN $T^{(j)}$ AND $X^{(j)}$

In this appendix we derive some useful relations to convert a typical vertex function to correlation functions. The starting expression is based on Eqs. (22) and (30), and written here schematically,

$$T = I + I[GG + IGG + IGGIGG + \ldots]I = I + IX^{(2)}I.$$

In effective interactions, this expression is joined by four lines, either G or connecting to the correlation functions $X^{(j)}$. In either case, one can use the vertex function Γ to explicitly multiply T by G,

$$GGTGG = P - GG.$$

When connected to one or more $X^{(j)}$, the derivative of T with respect to G, absorbs the connected correlation in defining the derivative of T with respect to U via the chain rule. We need only up to two derivatives in our formalism. They are

$$\frac{\delta T}{\delta U} = I^{(3)}X^{(2)} + I^{(3)}X^{(2)}X^{(2)}I^{(2)} + I^{(2)}X^{(2)}X^{(2)}I^{(3)} + I^{(2)}X^{(3)}I^{(2)},$$

$$\begin{aligned} \frac{\delta^2 T}{\delta U \delta U} &= I^{(4)}X^{(2)}X^{(2)} + I^{(3)}X^{(3)} + I^{(2)}X^{(3)}I^{(2)} + I^{(2)}X^{(4)}I^{(2)} \\ &\quad + \{I^{(3)}X^{(2)}X^{(2)}I^{(2)}\} + \{I^{(4)}X^{(2)}X^{(2)}X^{(2)}I^{(2)}\} \\ &\quad + \{I^{(2)}X^{(2)}X^{(2)}X^{(2)}I^{(4)}\} + \{I^{(3)}X^{(3)}X^{(2)}I^{(2)}\} \\ &\quad + \{I^{(3)}X^{(2)}X^{(3)}I^{(2)}\}, \end{aligned}$$

where the $\{\cdot\}$ indicate that the expression is to be symme-

trized by taking all permutations with $I^{(j)}$ always on the outside. The functionals $\delta T/\delta U$ and $\delta^2 T/\delta U \delta U$ generate integral kernels for $X^{(3)}$ and $X^{(4)}$ in the sense that they are amputated diagrams of the corresponding correlation functions obtained by cutting correlation functions joined to effective interactions. To see this write

$$GG\frac{\delta T}{\delta U}GG = \frac{\delta P}{\delta U} - PG - GP - PGTG - GPTG - GGTPG - GGTGP.$$

Each of the terms being subtracted are either explicitly unconnected, or they contain a P joined to a fully connected four-point function by just one leg. Since P begins at GG, this again contains an unconnected piece implicitly and is therefore not fully connected. In this manner all explicitly and implicitly unconnected diagrams are subtracted and the remaining six-point function, after amputating, represents the connected kernel for $X^{(3)}$.

APPENDIX E: DERIVATION OF EOM FOR $\mathfrak{X}_n^{(2)}$

Here we derive the integral form of the equation of motion for $\mathfrak{X}_n^{(2)}$, which is converted to differential form in the text. It is convenient to begin with the BSE Eq. (25). Suppressing the arguments of all the functions involved, we write

$$P = P^0 + P^0 I^{(2)} P,$$

where $P^0 = GG$ is the noninteracting correlation function. We now substitute $P = P_Q + \mathfrak{X}_n^{(2)}$, $I^{(2)} = I_Q^{(2)} + \Delta I_n^{(2)}$, and $P^0 = P_Q^0 + P_n^0$, where

$$P_n^0 \equiv [\mathfrak{X}_n^{(1)} G_Q + G_Q \mathfrak{X}_n^{(1)}].$$

Using the relationship,

$$P = GG + GGTGG, \tag{E1}$$

the BSE now takes the form

$$\mathfrak{X}_n^{(2)} = P_Q^0 I_Q^{(2)} \mathfrak{X}_n^{(2)} + P_n^0 \Gamma_Q + P_Q^0 \Delta' I_n^{(2)} P_Q + \mathcal{S}_n^{(2)},$$

where $\Delta' I_n^{(2)}$ consists only of nth order correlation functions, and all combinations of correlation functions of order lower than n in the field are subsumed into the *source term*, $\mathcal{S}_n^{(2)}$, which we write in integral form without the superscript l. Substituting Eq. (E1) evaluated at quasiequilibrium in the third term,

$$\mathfrak{X}_n^{(2)} = P_Q^0 \Gamma_Q^{(2)} \mathfrak{X}_n^{(2)} + P_n^0 + [P_n^0 I_Q^{(2)} + P_Q^0 \delta_n' I^{(2)}] P_Q^0 \Gamma_Q + \mathcal{S}_n^{(2)}.$$

The third term in the above equation can be rewritten using the variation of $P^0 I^{(2)}$ with only n-order correlation functions. To do this we write $P_Q^0 = P_Q^0 + P_n^0 - P_n^0$ in the term multiplying square brackets. Thus

$$[P_n^0 I_Q^{(2)} + P_Q^0 \Delta' I_n^{(2)}] P_Q^0 \Gamma_Q = [\Delta' I_n^{(2)r} - P_Q^0 I_Q^{(2)} P_n^0] \Gamma_Q.$$

On the right-hand side we have introduced the two-particle reducible interaction

$$I^{(2)r}(14;23) = P^0(12';21') T^{(2)}(1'4';2'3') P^0(3'4;4'3), \tag{E2}$$

which is diagrammatically the same as $I^{(2)}$ in Fig. 3, but the extra quasiparticle lines convert each T into $P - P^0$ [see also Fig. 6(a)]. There are also many terms arising from the products of lower order correlation functions, which we will pick up in the section on sources. These terms describe the contribution of local field corrections to the driving of the deviations. We now have the following integral equation with arguments of the functions restored,

$$\begin{aligned}\mathfrak{X}_n^{(2)}(14;23) &= P_n^0(14;23) + P_Q^0(14';23') I_Q^{(2)}(3'2';4'1') \mathfrak{X}_n^{(2)}(1'4;2'3) \\ &\quad + [\Delta' I_n^{(2)r}(14';23') - (P_Q^0 I_Q^{(2)})(12';21') P_n^0(1'4';2'3')] \\ &\quad \times \Gamma_Q(3'4;4'3) + \mathcal{S}_n^{(2)}(14;23).\end{aligned} \tag{E3}$$

The interpretation of the terms is the same as in the original equation. The first is the field induced changes in the free-particle propagation, while the second defines an effective two-particle potential. The third term represents field-induced changes in this potential. It consists of two terms, where the first describes these changes by $\mathfrak{X}_n^{(1)}$ and $\mathfrak{X}_n^{(2)}$, and the second removes those effects due to free-particle propagation that are contained by $\mathfrak{X}_n^{(2)}$ but already included by the first two terms in the equation.

APPENDIX F: DIAGRAM RULE 4

In this section we derive the diagram rules 4 and 5 in Sec. IV.

Rule 4. From the definition (40) of $\mathfrak{X}_n^{(j)}$,we note that it corresponds to differentiating $X^{(j)}$ n times with respect to the external two-point fields. The differentiation converts each constituent $X^{(i)}$ into $X^{(i+1)}$, where the two new arguments of the correlation function occur in pair and belong to the same function U. Thus each correlation is promoted to $X^{(i+1)}$, and then the new pair of arguments is contracted with an external field line. Since this is done separately for each correlation, no two separate correlation functions are allowed to be connected to the same U. This can also be interpreted as a rule to prevent overcounting. Two individual components connected by a field line form a contribution of the same field order to a lower particle order correlation function. Therefore they have been included in the equation for the corresponding function already.

The exception to this rule for the pulse that fully contracts a diagram is due to the fact that this contraction corresponds to lowering of the particle order of correlation, rather than a deviation in it. This pulse produces a two-point function after two arguments of the correlation functions evolving to that point are contracted. It takes $\mathfrak{X}_n^{(2)} \to \mathfrak{X}_{n+1}^{(1)}$ via the products of the form $\mathfrak{X}_n^{(2)}(1a;2a')U(a'a)$. From Fig. 4, it becomes clear that a, a' can exist on separate correlation functions. The rule is also equivalent to the statement that U occurs explicitly only in the equation for G, and is implicit in equations for all $X^{(2\ldots)}$ via $G[U]$.

*kvirk@physics.utoronto.ca
†sipe@physics.utoronto.ca

[1] X. Li, T. Zhang, C. N. Borca, and S. T. Cundiff, Phys. Rev. Lett. **96**, 057406 (2006).
[2] I. Kuznetsova, P. Thomas, T. Meier, T. Zhang, X. Li, R. Mirin, and S. Cundiff, Solid State Commun. **142**, 154 (2007).
[3] L. Yang, I. V. Schweigert, S. T. Cundiff, and S. Mukamel, Phys. Rev. B **75**, 125302 (2007).
[4] S. T. Cundiff, Opt. Express **16**, 4639 (2008).
[5] R. Boyd, *Nonlinear Optics* (Academic, New York, 2003).
[6] W. Schäfer and J. Treusch, Z. Phys. B: Condens. Matter **63**, 407 (1986).
[7] M. Z. Maialle and L. J. Sham, Phys. Rev. Lett. **73**, 3310 (1994).
[8] V. Axt and A. Stahl, Z. Phys. B **93**, 195 (1994).
[9] M. Kira and S. Koch, Prog. Quantum Electron. **30**, 155 (2006).
[10] R. Binder and S. Koch, Prog. Quantum Electron. **19**, 307 (1995).
[11] K. S. Virk and J. E. Sipe, Phys. Rev. B **76**, 035213 (2007).
[12] E. Blount, in *Solid State Physics: Advances in Research and Applications*, edited by F. Seitz and D. Turnbull (Academic, New York, 1962), Vol. 13, pp. 305–373.
[13] I. Souza, N. Marzari, and D. Vanderbilt, Phys. Rev. B **65**, 035109 (2001).
[14] G. Baym, Phys. Rev. **127**, 1391 (1962).
[15] N. Bickers, D. Scalapino, and S. White, Phys. Rev. Lett. **62**, 961 (1989).
[16] G. Baym and L. Kadanoff, Phys. Rev. **124**, 287 (1961).
[17] D. Kremp, M. Schlanges, and W.-D. Kraeft, *Quantum Statistics of Nonideal Plasmas* (Springer-Verlag, Berlin, 2005).
[18] R. Zimmermann, *Many-Particle Theory of Highly Excited Semiconductors* (Teubner-Texte zur Physik, Leipzig, 1987).
[19] J. Negele, *Quantum Many-Particle Systems* (Addison-Wesley Publishing Company, Reading, 1988).
[20] K. B. Ferrio and D. G. Steel, Phys. Rev. Lett. **80**, 786 (1998).
[21] R. A. Smith, Phys. Rev. A **46**, 4586 (1992).
[22] A. Jackson and R. Smith, Phys. Rev. A **36**, 2517 (1987).
[23] T. Bornath, D. Kremp, and M. Schlanges, Phys. Rev. E **60**, 6382 (1999).
[24] Note that the operators in the expectation value may have differentreal-time arguments.
[25] J. Sipe, J. Opt. Soc. Am. B **4**, 481 (1987).
[26] J. Sipe, Surf. Sci. **105**, 489 (1981).
[27] J. Jackson, *Classical Electrodynamics* (John Wiley and Sons, Inc., New York, 1999), Chap. 16.